



Physical Properties of Novel Two-dimensional Materials and Their Modifications

From first-principles studies



Yierpan Aierken

Supervisor: Prof. François M. Peeters

Advisor: Dr. Ortwin Leenaerts
Dr. Deniz Çakır

Department of Physics, University of Antwerp

This dissertation is submitted for the degree of
Doctor of Philosophy

Antwerp, Belgium

May 2017

Draft - v1.0

Tuesday 30th May, 2017 – 17:32

*I would like to dedicate this thesis
to my loving parents Arkin and Perwin,
to my beloved wife Adila Dilshat,
to my cherished sons Efran and Wildan.*

Draft - v1.0

Tuesday 30th May, 2017 – 17:32

Declaration

I hereby declare that except where specific reference is made to the work of others, the contents of this dissertation are original and have not been submitted in whole or in part for consideration for any other degree or qualification in this, or any other university. This dissertation is my own work and contains nothing which is the outcome of work done in collaboration with others, except as specified in the text and Acknowledgements. This dissertation contains fewer than 65,000 words including appendices, bibliography, footnotes, tables and equations and has fewer than 150 figures.

Yierpan Aierken

May 2017

Draft - v1.0

Tuesday 30th May, 2017 – 17:32

Acknowledgements

And I would like to acknowledge ...

Draft - v1.0

Tuesday 30th May, 2017 – 17:32

Abstract

This is where you write your abstract ...

Draft - v1.0

Tuesday 30th May, 2017 – 17:32

Table of contents

List of figures	xv
List of tables	xvii
1 Introduction	1
1.1 Graphene	3
1.1.1 History	3
1.1.2 Physical properties	5
1.2 Post-graphene materials and their general properties	6
1.2.1 Functionalized graphene	7
1.2.2 Group IV 2D materials	8
1.2.3 2D from layered materials	10
1.3 1D from 2D: nanotubes and nanoribbons	12
1.4 Synthesis methods	14
2 Computational methods	19
2.1 Theory	19
2.1.1 Density Functional Theory	19
2.1.2 Exchange-correlation functional	22
2.2 Implementation	25
2.2.1 Software Packages	28
3 General physical properties 2D materials	29
3.1 Structural properties	29
3.1.1 Layer structure	29
3.1.2 sp hybridization	32
3.2 Electronic properties	34
3.2.1 Example: graphene	34
3.2.2 Dirac cone and symmetry	36

3.2.3	Polar bond	36
3.2.4	Accurate description from DFT	36
3.3	Vibrational properties	36
3.3.1	Example: monolayer MoS ₂	38
3.3.2	Dynamic stability from phonon dispersion	39
3.4	Mechanical properties	40
3.4.1	Elastic and engineering constants	41
3.4.2	Mechanical stability: Born stability criteria	41
4	Results of Physical Properties Calculations in Novel 2D materials	43
4.1	Thermal properties	44
4.1.1	Thermal expansion and anharmonic oscillations	44
4.1.2	Quasi-harmonic approximation	44
4.1.3	Helmholtz free energy and specific heat	44
4.2	Piezoelectric properties	44
4.2.1	Piezoelectric constants	44
4.2.2	Importance of internal relaxation	44
4.3	Carrier transport properties	44
4.3.1	Carrier mobility	44
4.3.2	Deformation potential theory: non-polar materials	44
4.3.3	Deformation potential theory: polar materials	44
4.4	Magnetic properties	44
4.4.1	Magnetic ordering	44
4.5	Battery related properties	44
4.5.1	Principle of Lithium battery	44
4.5.2	Key quantities and their modelling	44
5	Results of Physical Properties Modification in Novel 2D materials	45
5.1	Number of layers and types of stackings	46
5.1.1	Electronic properties	46
5.1.2	Vibrational properties	46
5.2	Mechanical strain	46
5.2.1	Carrier mobility	46
5.2.2	Magnetic properties	46
5.3	Adatom adsorption	46
5.3.1	Electronic properties	46
5.4	Heterostructures	46

Table of contents	xiii
5.4.1 Electronic properties	46
5.4.2 Li diffusion	46
5.5 Defect induction	46
5.5.1 Structural properties	46
5.5.2 Electronic properties	46
5.5.3 Magnetic properties	46
6 Conclusions	47
References	49
Appendix A Appendix	59

Draft - v1.0

Tuesday 30th May, 2017 – 17:32

List of figures

1.1	Graphene publications	2
1.2	Relation of graphite, graphene, fullerene and nanotube. Image source: the Nobel prize in physics 2010 [4].	4
1.3	Graphene lattice and band structure.	6
1.4	Atomic and electronic structure of graphane	8
1.5	Graphite fluoride to fluorographene. Image source:[46]	8
1.6	Buckled hexagonal crystal structures of 2D group IV materials (X = Si, Ge, and Sn). Different colors represent different 2D planes and their distance is the buckling parameter δ . Image adapted from:[51]	9
1.7	Layered hexagonal crystal structures of BN. Image adapted from:[65]	11
1.8	Layered structures of TMDs	11
1.9	Band structure evolution of MoS ₂ from bulk to single layer. Image source: [78]	12
1.10	Chiral vector and different type of nanotubes. Image adapted from [79] . . .	13
1.11	Graphene production setups. Image source [84]	15
1.12	Growth of graphene on SiC wafer. Image source [87]	16
1.13	A ultra-large-area graphene film. Image source [89]	17
2.1	Comparison of the accuracy and the size of electronic structure calculation methods. Image source: [93].	20
2.2	Jacob's ladder for DFT approximations. Image source: [99].	24
2.3	MAE of the equilibrium lattice constants and band gaps of different functionals on SC40 solid test set. Data source: [102].	24
2.4	Schematic illustration of the relation between E_g and E_g^{KS} . Image adapted from: [104].	26
3.1	Energy-momentum dispersion relation of single layer and bilayer graphene as plane intersections of 3D graphite dispersion. Image adapted from: [115]. . .	30

3.2	Energy-momentum dispersion relation of single layer and bulk graphene as plane intersections of 3D graphite dispersion. Image adapted from: [117].	31
3.3	Three types of sp hybridizaton. Image adapted from: [119].	33
3.4	The formation of $sp^2 \sigma$ and $p_z \pi$ double bond. Image source: [121].	35
3.5	Graphene lattice and its Brillion zone. Image source: [14].	35
3.6	Possible positions of second atom (blue area) to guarantee the existence of Dirac cones as going from (a) square lattice to (f) hexagonal lattice. The first atom is located at the corners of the unit cell. Image source: [124].	36
3.7	(a) phonon modes of bulk (first row) and monolayer MoS ₂ at Γ q point. (b) phonon dispersion and DOS of monolayer MoS ₂ . Image adapted from: [127].	38
3.8	Imaginary frequencies shown as negative frequencies in a phonon dispersion plot.	39
3.9	(a) A structure at the convex (left) and concave (right) of the PES. (b) Searching for stable structure (phase transition).	39

List of tables

Draft - v1.0

Tuesday 30th May, 2017 – 17:32

Chapter 1

1

Introduction

2

A new field of research related to both material science and condensed matter physics has been formed since the synthesis of graphene in 2004 [1, 2]. Graphene is a sheet of carbon atoms in a crystal form having a single atom thickness. Given the thin plane-like structural nature of this type of materials the field is named two-dimensional (2D) material. The synthesis itself together with the phenomenal properties of graphene has leaded to a Nobel Price in physics rewarded to Andre Geim and Konstantin Novoselov in 2010 [3]. Since then, the field is expanding with the involvement of researchers not only from young community, but also from experts who have been working on graphene-related materials like graphite, fullerenes and carbon nanotubes. As a result, researches focused on graphene and related topics increasing with unprecedeted speed, see Fig. 1.1. While a part of these effects has been making to explore more on the graphene itself and its applications, the other parts were put on discovering new 2D materials like graphene. It has been evidenced from graphene, same material having different dimensionality can have different properties. Therefore, many materials with hidden properties which will only manifest themselves at other dimensions yet to be discovered.

3

4

5

6

7

8

9

10

11

12

13

14

15

16

On the other hand, with the advent of powerful supercomputer facilities, calculations that seems impossible to finish in a reasonable time now has been made possible. The accuracy of such calculations is the most crucial aspect of computational physics, especially when the results are utilized to predict the real materials properties. To make the time spend on costly supercomputer valuable, researchers and programmers have been making important progress to make sure theories and its implementation are correct and the results they yield are within acceptable precision. Equipped with these tools, theoretical predictions have served well on discovering unexplored properties and applications of the materials. Moreover, detailed characterizations at atomic scale benefits the experimental results as well, or even to explain the unexpected outcomes.

17

18

19

20

21

22

23

24

25

26

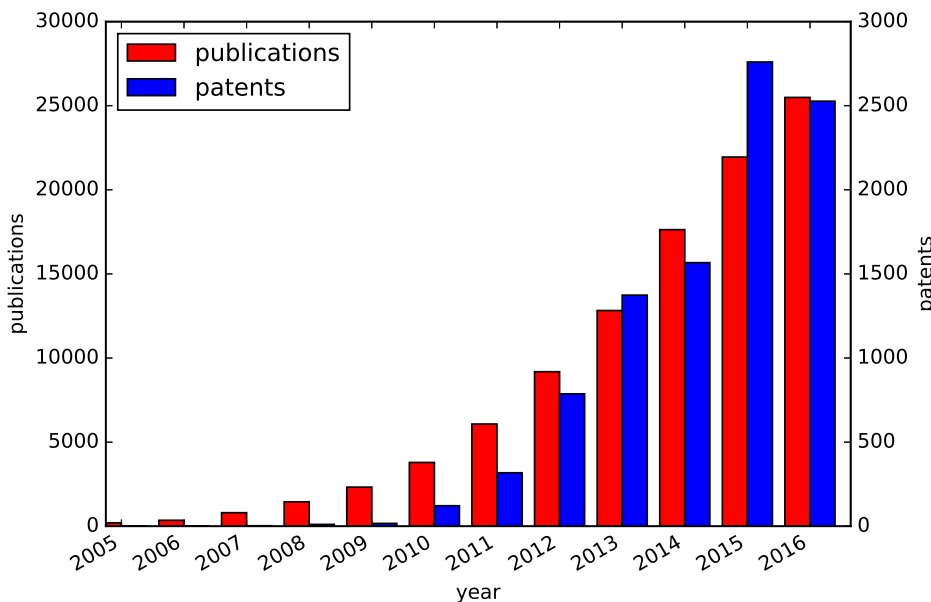


Fig. 1.1 Graphene related publications and patents during the last decade. Data source: ISI Web of Science and PATENTSCOPE.¹

Considering all mentioned, it is a sound approach to apply the state-of-the-art computational methods that accompanied with high-performance supercomputer facilities to investigate the physical properties of novel 2D materials. This thesis were initiated to this end and it is a summary of several works which has been accomplished during my PhD study. The thesis is organized as followed: For the rest of this chapter, I will first introduce graphene and some post-graphene materials that discovered right after graphene and, briefly, several well-known methods used to synthesis 2D materials. The following [chapter 2](#) will present the computational methods, the theory and the implementations of them in available software packages. In [chapter 3](#), I will discuss several general properties of 2D materials. The next two chapters will be the main results from my works. Starting from specific properties targeting at specific novel 2D materials in [chapter 4](#), and followed by modification of physical properties of 2D materials in [chapter 5](#). Overlaps of materials themselves and their properties are inevitable between sections yet it will be minimized, such that each section will have a unique topic.

¹Publication and patent results are obtained by searching for "graphene" in the topic field of Web of Science and the title field of PATENTSCOPE, respectively.

1.1 Graphene

Graphene is composed of carbon (C) atoms arranged on a honeycomb lattice in a single atomic layer. Graphene is one of layers that construct graphite, see Fig. 1.2. These layers in graphite are stacked on top of another through weak physical bonding, whereas within each layer C atoms are hold together by strong chemical bonding. As a result, it is possible to just isolate single layer from graphite without damaging the layer itself.

1.1.1 History

The story of graphene can be traced back to the discover of graphite around 1564 in England[5]. Ever since, people have been using the graphite, the tip of a pencil, for writing and drawing. The black trace left behind by pencil they are actually stacks of graphite and graphene, by chance even a single layer graphene can present. Apart from being a part of a pencil, graphite certainly has been holding a more important position in technology and industry due to its rich chemistry, low friction, high electrical and thermal conductivity etc. . On the other hand, the synthesis of single layer graphene seems to be discouraged by both experimental and theoretical limitation. On the experiments, there have been attempts[6, 7, 8, 9] to isolate graphene from graphite or even grow it on a substrate. However, they were mostly failed on the control of the number of layers and identifying graphene itself. Addition to these experimental difficulties, on the theory, it was believed that strictly 2D material should not exist due to a divergence in the thermal fluctuation in 2D materials that will make them not stable [10, 11, 12]. Nevertheless, graphene was still considered as a theoretical model. for example, Wallace [13] was the first one to study the band structure of graphene [14] and found some of the interesting properties like semimetallic band structure.

Although not in the form of graphene, the single atomic layer of graphite has been already seen and studied in other forms, e.g. fullerenes and nanotubes, see Fig. 1.2. These material usually contain certain types of characteristic defects that differ it from graphite. Fullerene is a C molecule has a quasi-spherical hollow ball shape. It is composed of both six- and five-folded C rings, where the latter give positive curvature and made closed surface possible. The resulting shape resembles a football[15, 16]. The Nobel prize in chemistry of year 1996 was award to Harold W. Kroto, Robert F. Curl and Richard E. Smalley for their discovery of fullerene. Another important type of carbon allotrope, carbon nanotubes[17], was discovered using arc-discharge method[16] which was originally designed to produce a large quantity of fullerenes. Despite sharing similar production method, carbon nanotubes are actually more close to graphene than fullerene due to the absence of pentagonal C rings in the former two. A carbon nanotube can be construct by rolling up graphene sheet into a hollow tube as its name

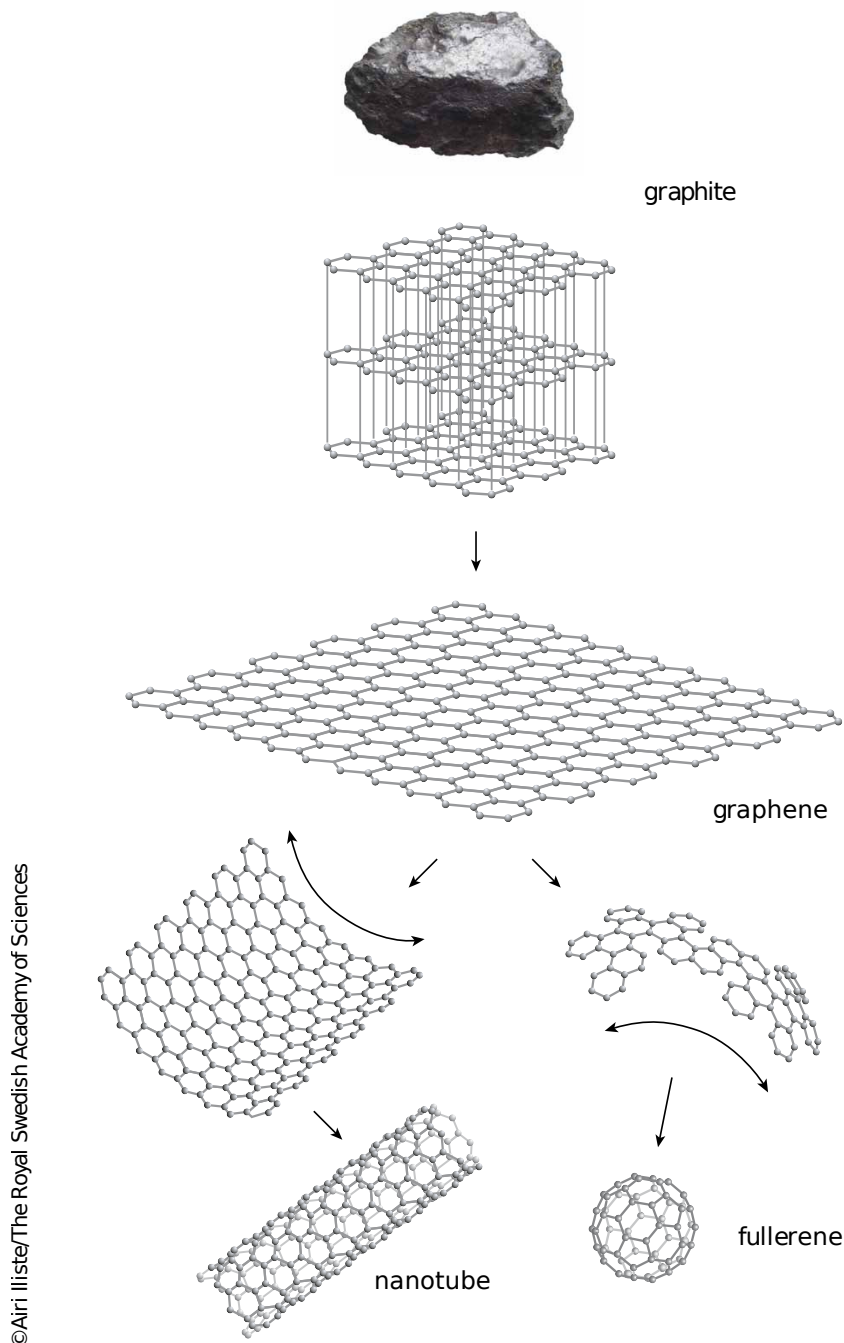


Fig. 1.2 Relation of graphite, graphene, fullerene and nanotube. Image source: the Nobel prize in physics 2010 [4].

1.1 Graphene

5

suggested. Carbon nanotubes are observed to have micrometer in lengths and nanometre in diameters and having either metallic or semiconducting nature depending on its edges. They possess superior mechanical properties. Individual nanotube has a Young's modulus of 0.64 TPa and it is 56 times stronger than steel wire[18].

In 2004, the situation has changed completely for graphene with the successfully isolated single layer graphene from graphite by A. K. Geim and K. S. Novoselov at Manchester University using a simple micromechanical cleavage method. The key ingredient for success in this case as compared to the previous failures[6, 7], except for the sophisticated experimental control, is that the Si wafer under the graphene made it easier to identify graphene[3]. The synthesis of graphene itself already is a ground-breaking achievement, however, what excited the researcher the most is the extraordinary properties of graphene. In the following section, I will summarized some of them to illustrate this point.

1.1.2 Physical properties

As mentioned previously, graphene is the single atomic layer of graphite. It posses an interesting structure with high symmetry which many of its properties are attributed to. Each C atom has three neighbours to make chemical bonds. Because of this, C atoms are arranged in a honeycomb lattice², or a hexagonal Bravais lattice with two atoms per site, see (a) in Fig. 1.3. Graphene has uniform bond lengths of 1.42Å and uniform bond angles of 120°. The band structure which characterizes the electronic properties of graphene has been calculated by P. R. Wallace in 1947 [13]. He discovered that graphene is a semimetal with conduction band minimum (CBM) and valence band maximum (VBM) only touch each other at the K and K' points in the first Brillouin zone as shown in (b) and (c) in Fig. 1.3. The energy-momentum dispersion is approximately linear in the vicinity of K and K' points. Due to this, the electron and hole in those states behave differently as they do in quadratic band. Several consequences of this can be concluded. First of all, considering the linear energy momentum relation, particles can be regard as Dirac particles and they are governed by relativistic Dirac equation[19], and they travel at constant speed of 10⁶m/s. Hence, the K and K' points are referred as Dirac points, their vicinities are called Dirac cones. Secondly, the carrier concentration can be tuned continuously from electron to hole with a perpendicular electric field[3]. Thirdly, the carrier in graphene can tunnel through finite height potential it normally incident to without reflection — Klein tunnelling[20]. Fourthly, under magnetic field, zero energy Landau level appears, and the large energy interval between zero to first level made it possible to observe quantum Hall effect at room temperature [21], etc..

²honeycomb lattice is not a Bravais lattice.

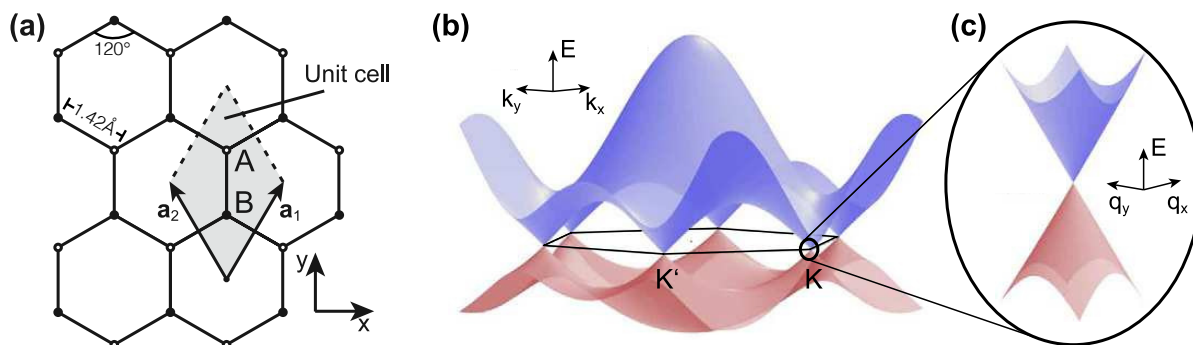


Fig. 1.3 (a) Graphene honeycomb lattice composed of A and B hexagonal Bravais sublattices. (b) Band structure of graphene where CBM and VBM touch each other only at the K and K' points. (c) Approximately linear dispersion around the K and K' points. Image source: [22].

Graphene delivers more than just an interesting electronic property. For example, evidencing the extraordinary mechanical properties, graphene has a Young modulus $E = 1\text{ Tpa}$ and intrinsic strength of 130 Gpa [23]. This makes graphene the strongest material ever measured. More than 300 times stronger than steel and four times harder than diamond. Carrier high mobility is another exciting feature that has more applicative importance in electronic devices. Free standing graphene without substrate attached has been reported to have mobility of $230,000\text{ cm}^2/\text{Vs}$ at low temperature[24] and $120,000\text{ cm}^2/\text{Vs}$ at 240 Kelvin, the latter value is higher than any known semiconductor[25]. In addition, the thermal conductivity of graphene can reach up to 5000 W/mK at room temperature, which is 20 times higher than copper[26]. However, having a zero band gap means the application of graphene in digital logic gates is limited. The current controlled by the gate bias can not be turned off completely which would otherwise deliver distinct signal from when it is on. Efforts on band gap opening have been made, from substrate induction[27, 28], bilayer graphene[29, 30], chemical adsorption[31, 32], and chemical doping[33] to quantum confinements[34, 35]. While doping and adsorption usually come with a cost of reducing mobility by introducing scattering centres, chemically pure bilayer graphene and nanoribbon are thought to be promising approaches to open band gap as well as, to a great extent, preserve graphene's superior intrinsic properties.

1.2 Post-graphene materials and their general properties

Excitements in the exploration of graphene properties drive the force to discover more types of 2D materials. Researchers have taken different approaches to this end. On one hand, aiming to open a band gap in graphene, chemical functionalizations on graphene have been carried out with adsorption of hydrogen, fluorine and oxygen, and they results in graphane, fluo-

1.2 Post-graphene materials and their general properties

7

rographene and graphene oxide, respectively; On the other hand, inspired by graphite's layer structure, layered materials are brought to the attention to isolate its single layer just as it has done for graphene. In this section, I will introduce some of these early post-graphene materials and their physical properties in general.

1.2.1 Functionalized graphene

Graphane

The fully hydrogenation of graphene gives a 2-D hydrocarbon called graphane. It can synthesized either by reduction of graphite then hydrogenation of left product (graphene, carbon nanotubes or graphite oxide) with liquid-based[36] or gas-based[37] environments, or growing by chemical vapour deposition[38].

graphane is not flat as graphene. In fact, the bonding character changed from sp^2 hybridization to sp^3 , which gives buckled structure, see Fig. 1.4. Neighbouring H atoms locate at the different sides of graphane plane. Among different phases of graphane, chair structure is the ground state. Others phases are metastable state like: boat, twist-boat and twist-boat-chair[39]. The C-C bond length in the chair structure is 1.52 Å lager than that in graphene. graphane is a semiconductor with 3.5 eV band gap in the chair form. Band gap is reported scales almost linearly with the hydrogen coverage[40]. The 2D Young's modulus of graphane is estimated 245 N/m[41], smaller than 340 N/m in graphene. The incomplete coverage of H atoms on graphene gives hydrogenated graphene. It has ferromagnetic magnetic state[42], tunable band gap[43] and reversible hydrogenation[31].

Fluorographene

More stronger binding between external atom and C atom can be realized using fluorine atom for adsorption . A full fluorinated graphene is called fluorographene, and it can be regards as a single layer of graphite fluoride. Actually, sonochemical exfoliation of fluorographene from graphite fluoride is one of the ways to synthesis it, see Fig. 1.5[46]. Fluorographene has a similar structure as graphane due to same sp^3 hybridization, and it also has different isomers where the again the chair type is the ground state configuration[47]. The unit cell of fluorographene is around 1% larger than that of graphene[48]. The formation energy of fluorographene is around 0.5 eV per fluorine atom lower than that of graphane per hydrogen atom[32]. The band gap of fluorographene is larger than 3 eV from optical measurement[48, 32], and band structure is similar to that of graphane with a band gap at the Γ k-points. The 2D Young's modulus of Fluorographene is 100 N/m and the intrinsic strength is about 15 N/m.

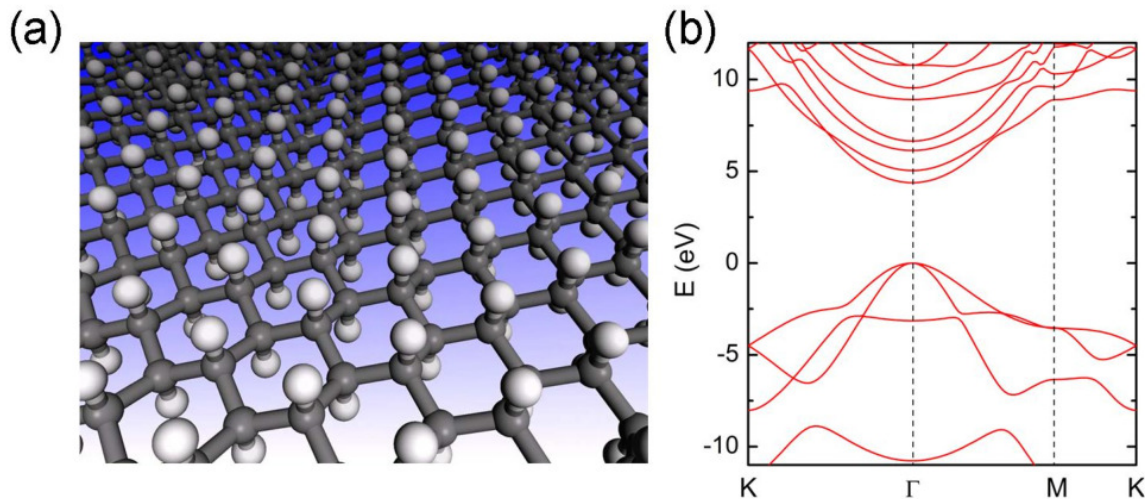


Fig. 1.4 (a)The chair structure of graphane. The white balls are the H atoms and the grey ones are the C atoms. Image source: [44]. (b) Band structure of chair graphane. Image source: [45]

¹ They both more than two times less than those for graphene due to weaker sp³ bonds in
² fluorographene[48].

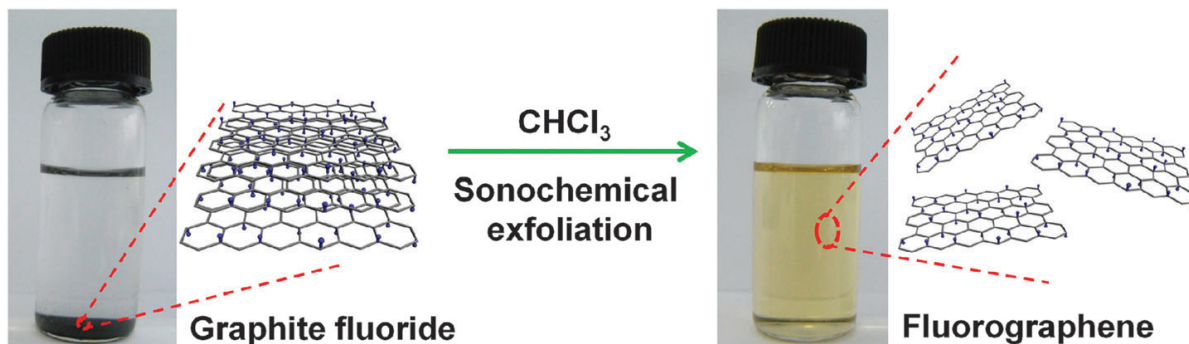


Fig. 1.5 Graphite fluoride to fluorographene. Image source:[46]

³ 1.2.2 Group IV 2D materials

⁴ In analogues to graphene, 2D material made of only single element from other members of
⁵ group IV have been also proposed and synthesized. They are silicene, germanene, stanene
⁶ made of silicon (Si), germanium (Ge) and tin (Sn) atoms, respectively. They generally suffer
⁷ from less stability with respect to graphene. The free standing form of these material are
⁸ hard to make, instead they usually need ordered substrates to support them. Therefore, the
⁹ measurements done on these type of system can not exclusively speak for the target mate-
¹⁰ rial, the influence of the substrate is not negligible[49]. This will in turns hinder the accurate

1.2 Post-graphene materials and their general properties

9

characterization of the properties. Despite these experimental difficulties, theoretical studies have more freedom to investigate their physical properties. One of the most important differences of these materials as compared to graphene is their not-flat buckled structure, see Fig. 1.6. The buckling parameters δ is defined as the interlayer distance of layers at different 2D atomic planes. According to calculations, δ is 0.45 Å for silicene, 0.69 Å for germanene and 0.85 Å for stanene[50]. This change corresponds to a more sp³ character in the orbitals, and it increases with the atomic radius.

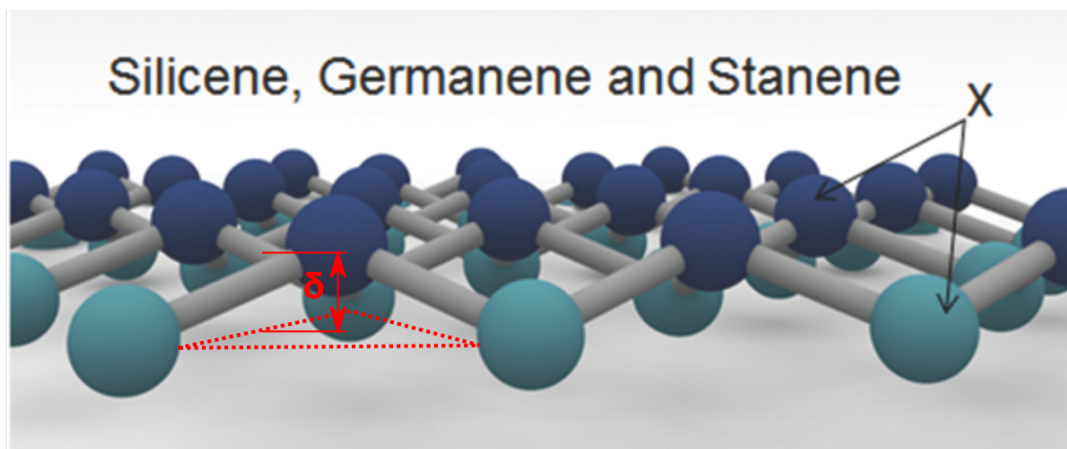


Fig. 1.6 Buckled hexagonal crystal structures of 2D group IV materials ($X = Si, Ge, and Sn$). Different colors represent different 2D planes and their distance is the buckling parameter δ . Image adapted from:[51]

Although having a buckled structure, these materials also posses Dirac points with linear energy momentum dispersion around it[52]. However, as stated before, the substrate where the materials are supported will induce symmetry broken which leads to the lost of Dirac character for particles[49]. Moreover, spin-orbit coupling (SOC) in these materials are predicted to be larger than that in graphene due to larger atomic weights. With inclusion of SOC, this corresponds to 1.9 meV band gap in silicene and 101 meV of that in stanene[50]. The mechanical stiffness and strength are low as compared to graphene and has a reducing trend with increasing atomic number in this group. This is partially due to the less energetically costly bond angle deformation in the buckled structure upon load rather than bond stretching in a flat structure[53]. For example, silicene has a 2D Young's modulus around 62 N/m, that is four times smaller than graphene. Another important difference of these materials from graphene regards the realization of monolayer. The lack of layered bulk materials for the former ones made the mechanical exfoliation inapplicable for them, which is believed to produce the highest quality sample otherwise. Therefore, methods used in this case are either bottom-

- 1 up decomposition techniques onto highly ordered substrates[54, 55], or top-down methods
- 2 like chemical exfoliation to isolate grown monolayer from substrate[56, 57].

3 **1.2.3 2D from layered materials**

4 The layered structure of graphite contribute the most to the isolation of graphene. If the
5 interlayer bonding were not weak vdW interaction rather a covalent type, even the concept
6 of layers can not stand let alone to break the bonds only in one direction and keep others in the
7 other two directions. Therefore, a reasonable way to explore other 2D materials is through
8 other layered materials, e.g. hexagonal boron nitrides, transition metal dichalcogenides. In
9 this section, I will discuss general physical properties of these two material as examples for
10 2D materials from layered materials.

11 **Boron Nitride**

12 Among the multiple structural phases of Boron Nitride, the layered hexagonal phase (h-BN) is
13 the most stable one, see Fig. 1.7 for the structure. A single layer extracted from it gives 2D h-
14 BN. Because of its structural similarity to graphene and its wide band gap it is often referred
15 as the white graphene[58]. 2D h-BN has a band gap of 6.1 eV according to calculations. A
16 intuitive tight binding analysis reveals the band gap, in the of 2D h-BN, is proportional to the
17 difference of p_z orbitals from B and N atoms. For silicene and graphene, this difference is
18 zero thus so is the band gap. Moreover, as a result of different electronegativity, i.e. 2.0 for
19 B and 3.0 for N, ionic character develops which further enlarge the band gap[59]. Several
20 interesting features of this material are reported: strong mechanical stiffness and strength
21 close to graphene[60], a good thermal conductivity of 100-270 W m⁻¹ K⁻¹ for few-layer h-
22 BN[61] as an electrical insulator, a high oxidation resistance up to 700 °C as contrast to 400 °C
23 for graphene[62], etc.. Benefit from its compatible bond length, i.e. 1. Å, with graphene, it is a
24 perfect partner for graphene to form heterostructure electronic device to serve as a dielectric
25 substrate[63], the result is reported better than using SiO₂ substrate[64] for instance.

26 **Transition Metal Dichalcogenides**

27 Transition metal dichalcogenides (TMDs) have a generalized formula of MX₂, where M stands
28 for the group 4-7 elements in the transition metal series in the periodic table, and X are the
29 group VI elements. This is another type of layered materials, and the single layer of some of
30 them have been experimentally realized. These materials typical exist in three different struc-
31 tural phases as shown in Fig. 1.8, which at monolayer level can be either H or T phase. One

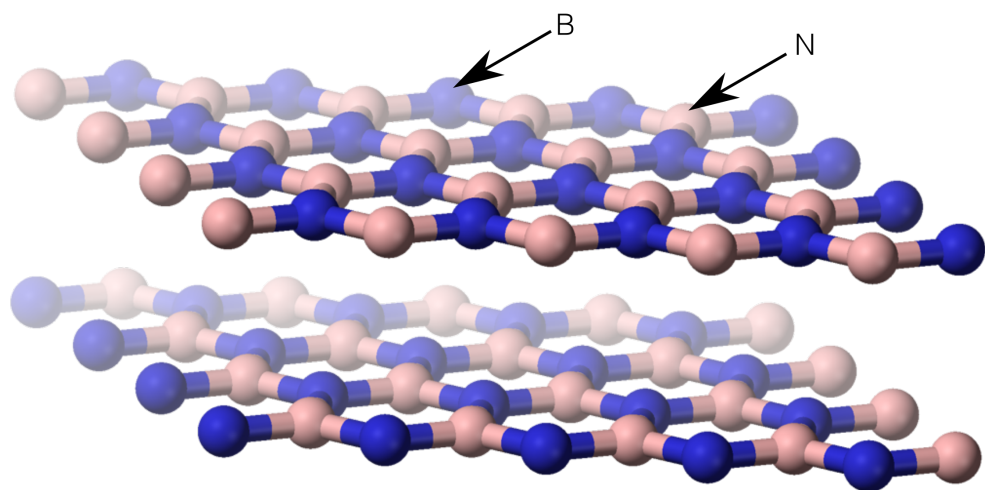


Fig. 1.7 Layered hexagonal crystal structures of BN. Image adapted from:[65]

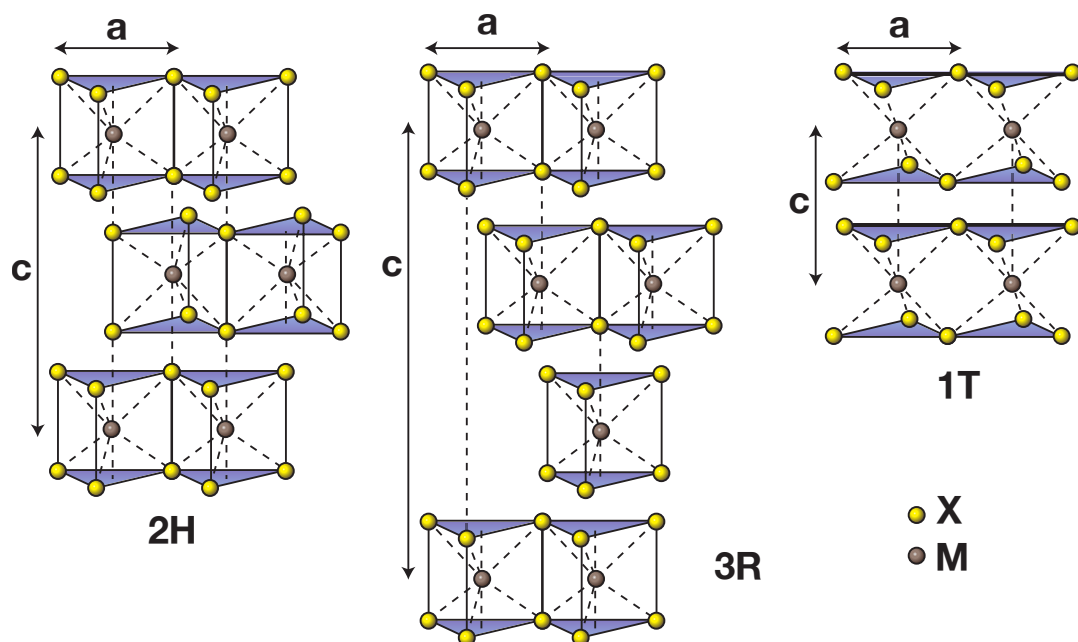


Fig. 1.8 Layered structures of TMDs. 2H: two layers per unit cell with hexagonal symmetry; 3R: three layers per unit cell with rhombohedral symmetry; 1T: one layer per unit cell with tetragonal symmetry. a is the in-plane lattice constant with a range from 3.1 to 3.7 Å in TMDs. c is the vertical lattice constant. The interlayer distance has a typical length of 6.5 Å. Image source: [66]

of the most important differences in these two phases is the lack of inversion symmetry in H phase while T phase has it. Therefore, spin orbit coupling (SOC) is much important in H to induce spin-splitting than that in T phase, for instance 456 meV spin splitting in WSe₂[67] has been reported. Note that, inversion symmetry is recovered in the layered bulk form hence suppresses SOC. Another important consequence of reduce dimensionality is the indirect-to-direct band gap transition from layered TMDs to its 2D counterpart, see for example in Fig. 1.9. 2D-TMDs have a broad range of potential applications. Electrocatalysis[68, 69] benefit from adequate active sites, electronic devices[70, 71] benefit from typical band gap of 1-2 eV, Li or Na batteries[72, 73] benefit from high surface-to-volume ratio and short diffusion path, photocatalysis benefit from high stability under extreme light intensity[74, 75], and biomedicine benefit from enhancement of the physiological stability and biocompatibility of polymers on 2D-TMDs[76, 77].

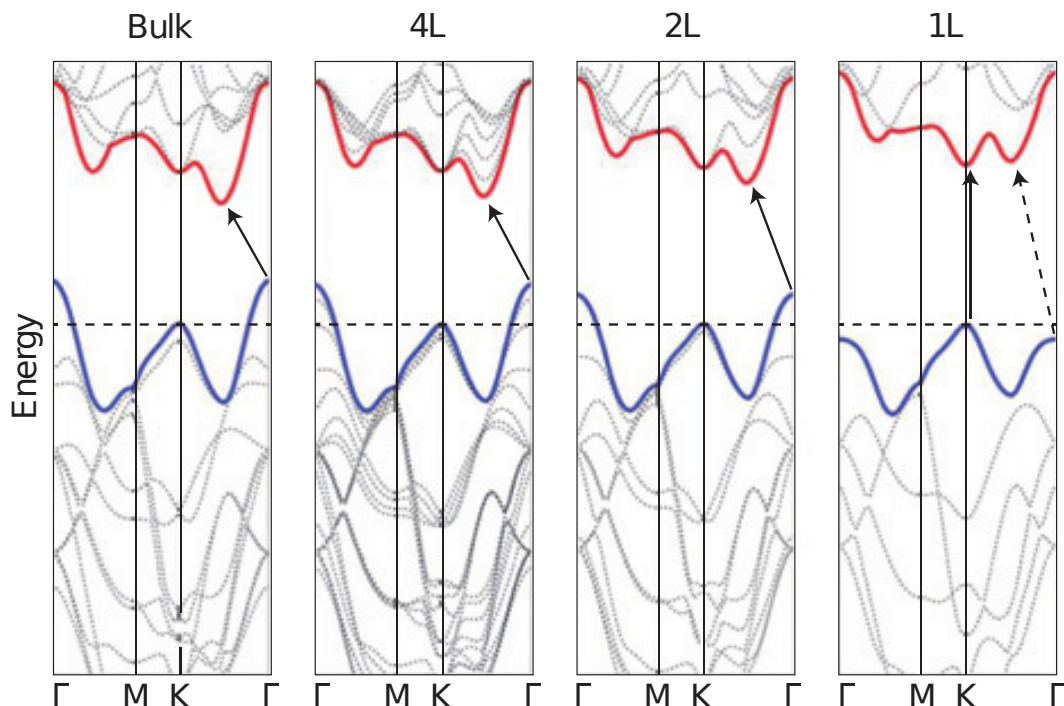


Fig. 1.9 Band structure evolution of MoS₂ from bulk to single layer. Image source: [78]

1.3 1D from 2D: nanotubes and nanoribbons

The reduction of dimensionality of the materials did not stop at the 2D level. Further lowering it will result in 1D nanotubes or nanoribbons.

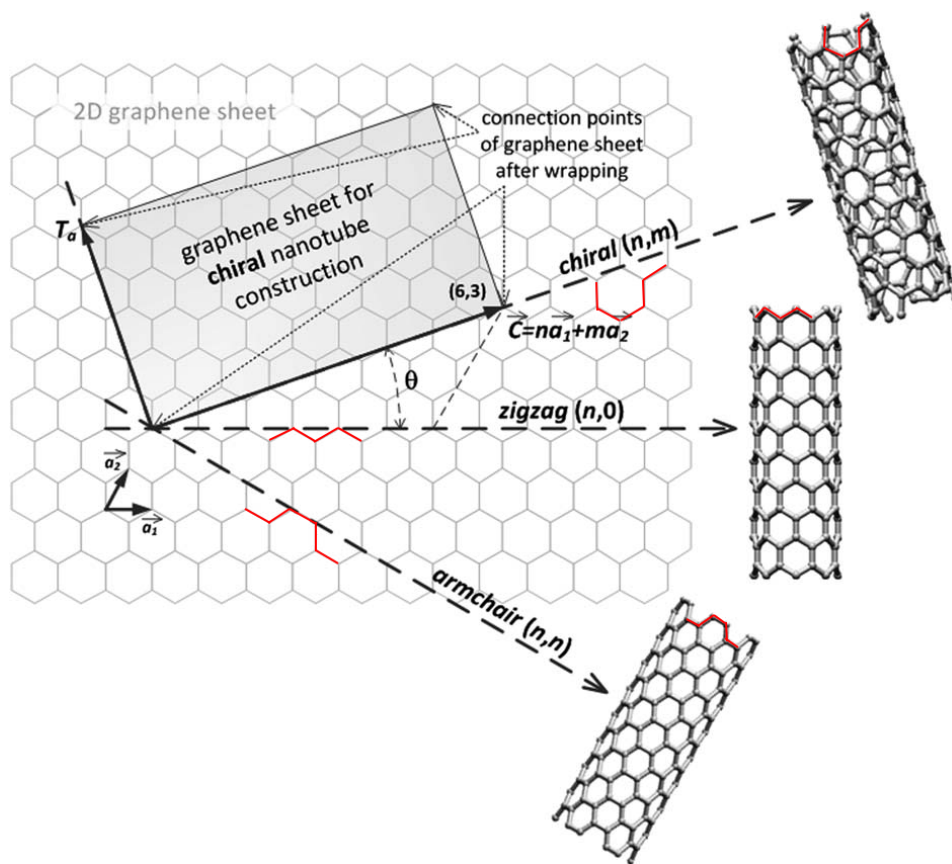


Fig. 1.10 Chiral vector and different type of nanotubes. Image adapted from [79]

1 A nanoribbon is a strip of 2D sheet with nano-scale width and micro-scale length and it is
2 still flat. Whereas nanotubes are the rolling up of nanoribbons to have a tube structure. Each
3 nanotube, also each nanoribbon but with different definition, is associate with a chiral vector
4 that uniquely define its structure parameters expect the length which is consider to be infinite
5 in theory. In the Fig. 1.10, a_1 and a_2 are the unit lattice vectors in graphene. Chiral vector, \vec{C} ,
6 is the superposition of these two unit vectors with indices pair (n,m) . Zigzag edge always has
7 a $(n,0)$ form and (n,n) is always armchair edge. Everything else is called chiral type edge. This
8 finite-length chiral vector also define the radius of the tube. Nanoribbons, on the other hand,
9 have these three types of edges as well. However, in this case, edges have infinite length.

10 With confinements from other directions, physical properties of these system are expected■
11 to be different than that in their higher dimension counterparts. For example, graphene
12 nanoribbons have a finite band gap as contrast to zero band gap in graphene[80]. More-
13 over, control of this confinement will give tunable physical properties. For example, overall
14 inverse band gap relation with the width of nanoribbon[81]. The zigzag edges in graphene
15 nanoribbon form spin-polarized magnetic states give ferromagnetic ordering along the edge
16 and anti-ferromagnetic ordering across edges[82]. For nanotubes, those have same edges be-
17 long to the same class of chirality and have same electronic structure. For instance, armchair
18 carbon nanotubes are metallic, other types are semiconducting. But small radius tubes can
19 be exceptional due to large curvature[83]. The strong mechanical strength and high thermal
20 conductivity of graphene nanoribbon similar to those in graphene.

21 1.4 Synthesis methods

22 In this last section, I will briefly discuss some of the well-known synthesis methods for 2D
23 materials. In Fig. 1.11, a overview of graphene production methods is displayed in Fig. 1.11.

24 Micromechanical cleavage

25 Micromechanical cleavage is also known as mechanical exfoliation, which was the method
26 used to first successful isolation of graphene in 2004 using a adhesive tape[2]. It involves
27 separating layers in layered materials by mechanical, electrostatic, or electromagnetic forces.
28 This method gives high quality product and suitable for laboratory-scale sample for fundamen-
29 tal studies. Large scale productions are impractical through this method. Room temperature
30 mobility was measured up to $20,000 \text{ cm}^2\text{V}^{-1}\text{s}^{-1}$ [85] on graphene prepared with this method.

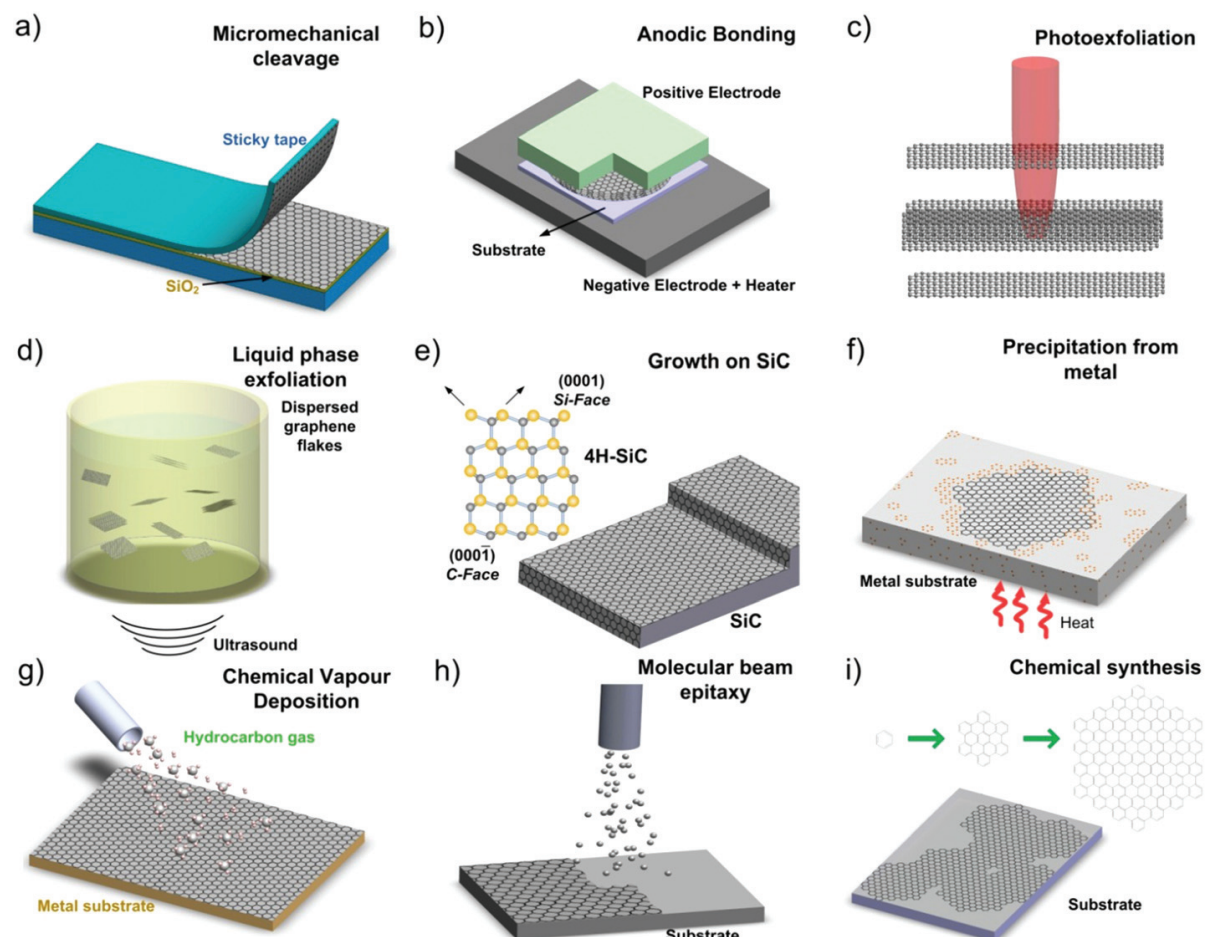


Fig. 1.11 Graphene production setups. Image source [84]

1 Liquid phase exfoliation

2 Liquid phase exfoliation is the extraction of layers in a proper solvent using ultrasounds. The
 3 cavitation-induced bubbles collapse around the graphite will generate compressive stress
 4 wave. As a primary result, this will cause a reflective tensile wave whose strength is propor-
 5 tional with the number of such bubbles. Intensive tensile stress is enough to break graphite
 6 into graphite flakes. Additionally, as a secondary effect, shear effect can be develop from un-
 7 balance lateral stress, and separate two adjacent layers. Liquid phase exfoliation is a promising
 8 method to synthesis cheap and scalable samples.

9 Growth on SiC

10 Growth of graphene on SiC involves SiC sample annealing at high temperature ($> 1400^{\circ}\text{C}$) in
 11 vacuum or under atmospheric pressure. The sublimation of silicon atoms leave behind carbon
 12 atoms on the surface which will rearrange to form graphitic layer[86], see Fig. 1.12. Apart from
 13 high reproducibility and production of homogeneous large-area sample of this method, it has
 14 an advantage that the graphene is available on semiconducting substrate for layer electronic
 15 device integration.

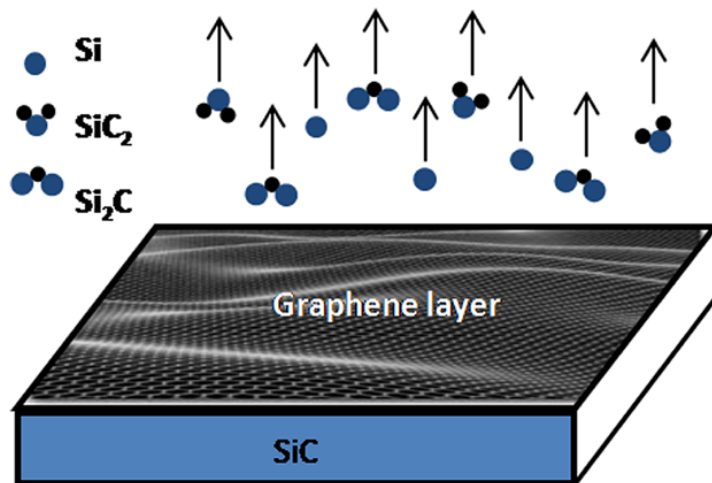


Fig. 1.12 Growth of graphene on SiC wafer. Image source [87]

16 Chemical vapor deposition

17 Chemical vapor deposition (CVD) is a popular method to grow amorphous or crystalline thin
 18 film from solid, gaseous or liquid precursors. It is a direct deposition of vaporized desire ma-
 19 terial onto a particular substrate. Various of CVD methods exist depending on their operating

pressure, types of vaporization and whether it is plasma-assisted etc.. Graphene grown on transition metals usually has a high quality. Carbon atoms from organic sources in the gas phase are deposited on metal (Ni, Ru, Ir etc.) and convert to graphene at high temperature. Then, for the characterization, graphene will be transferred to a proper substrate. Typical mobility of such type of sample is around $1000\text{-}25000\text{ cm}^2\text{V}^{-1}\text{s}^{-1}$ [88]. A 30-inch graphene film has been produced from roll-to-roll production through CVD methods by Bae et al. [89], see Fig. 1.13. The product measured to be a better electrode than commercially available indium tin oxides.

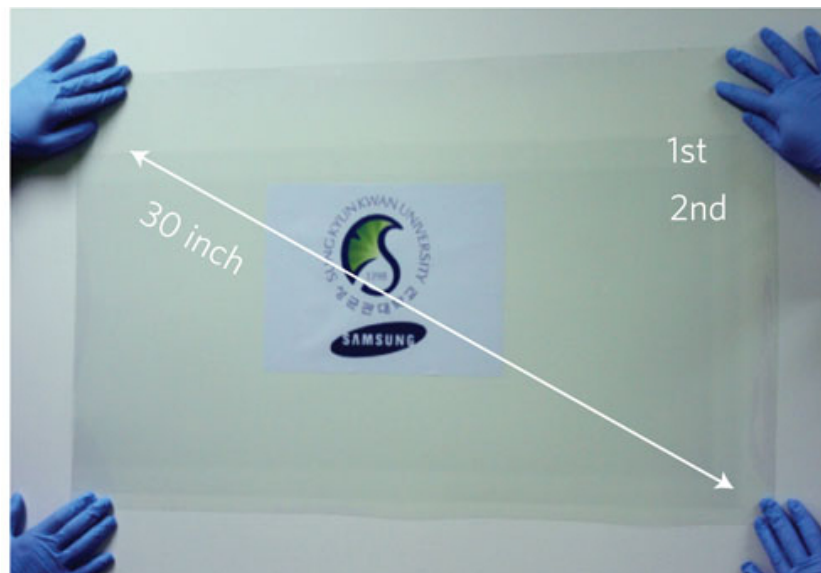


Fig. 1.13 A ultra-large-area graphene film. Image source [89]

Draft - v1.0

Tuesday 30th May, 2017 – 17:32

Chapter 2

Computational methods

As mentioned in the last chapter, theories behind the calculations are the core component in the material properties determination process. Its correctness, accuracy and implementation directly influence the quality of its predictions. In this chapter, I will introduce relevant theoretical models, approximations and their implementations in commonly used software packages.

2.1 Theory

2.1.1 Density Functional Theory

Density functional theory (DFT) is one of the most widely used quantum mechanical method to calculate the properties of materials. Its applicable length and time scale are in nanometre and picoseconds, respectively. This is longer than quantum Monte Carlo simulations and lower than semi- or full-empirical methods in both scales. This order is also valid in the accuracy verse size-of-the-system plot in Fig. 2.1. The accuracy can be higher than that in the plot, since a large part of the inaccuracy attributes to the uncertainty of the experimental results that the methods are compared with[90]. As I will discuss in the later section, if a DFT method is compared with a highly accurate theoretical benchmark method, DFT would have a precision around 1 meV/atom. For periodic bulk or nanostructure, DFT can be used to even quantitatively predict the properties of materials. DFT is based on two main basis: Hohenberg-Kohn theorems[91] and Kohn-Sham equations[92]. Here I will briefly overview these without putting too much stress on the derivation which have been extensively documented in textbooks.

Materials are made from electrons and nuclei. Type of nuclei and the interactions between these components give rise to various materials and their properties. The interactions

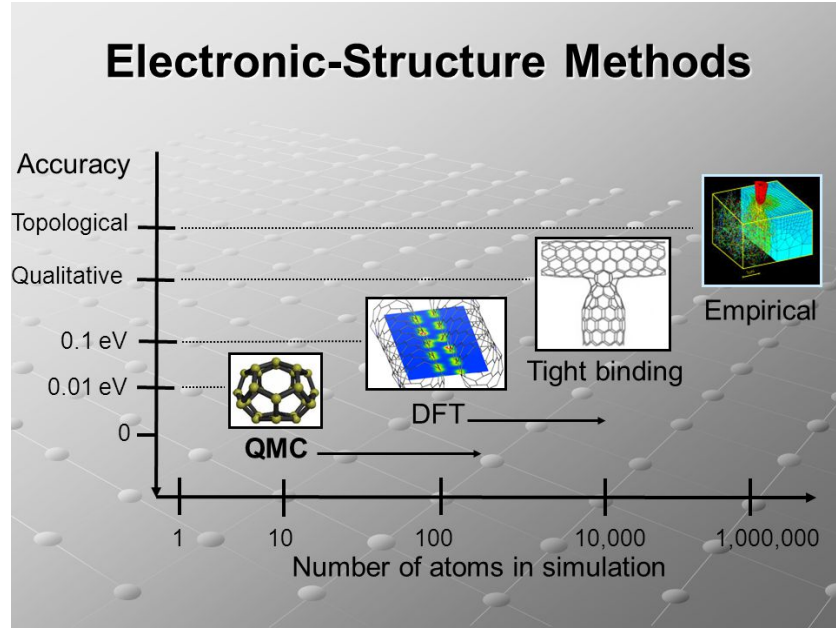


Fig. 2.1 Comparison of the accuracy and the size of electronic structure calculation methods.
Image source: [93].

- ¹ are mainly electrostatic or Coulombic. While electrons must be described with quantum mechanics, the nuclei can be treated as classical particles. The equation governing electron behaviour is the Schrödinger equation. It can be written as follows:¹

$$\begin{aligned} \hat{H}\psi_{\alpha}(\vec{r}_1\sigma_1, \dots, \vec{r}_N\sigma_N) &= \left[-\frac{1}{2} \sum_{i=1}^N \nabla_i^2 + \sum_{i=1}^N v(\vec{r}_i) + \frac{1}{2} \sum_{i=1} \sum_{j \neq i} \frac{1}{|\vec{r}_i - \vec{r}_j|} \right] \psi_{\alpha}(\vec{r}_1\sigma_1, \dots, \vec{r}_N\sigma_N) \\ &= (\hat{T} + \hat{V}_{ext} + \hat{V}_{ee}) \psi_{\alpha}(\vec{r}_1\sigma_1, \dots, \vec{r}_N\sigma_N) \\ &= E_{\alpha} \psi_{\alpha}(\vec{r}_1\sigma_1, \dots, \vec{r}_N\sigma_N). \end{aligned} \quad (2.1)$$

⁴ ⁵ ⁶ ⁷ ⁸ ⁹ ¹⁰ ¹¹ \hat{H} is the total Hamiltonian. \hat{T} is the kinetic energy. \hat{V}_{ext} is the interaction between electrons and nuclei. Here we already started with the first approximation: Born–Oppenheimer approximation[94]. Which neglect the dynamics of nuclei, instead electrons are considered moving in a static potential generated by their interaction with all nuclei. \hat{V}_{ee} is interaction between electrons. The first two sum over all N -electrons, and the last one sums over all unique pairs of N -electrons. \vec{r} is the electron position. σ is the z-component of spin on electron ($+\frac{1}{2}, -\frac{1}{2}$). ψ is the N -electron wave function, and it should be antisymmetric under interchange of

¹Equations in this chapter are written in cgs form, and the fundamental constants \hbar , e^2 and m are set to unity.

two electron orbital and spin coordinates (i.e. fermionic character for electrons) and it should also satisfy boundary condition of the system (e.g. quantum confinement for low-dimensional system). E is the total energy. α is the complete set of N -electron quantum numbers. Following constrained search algorithm introduced by M. Levy[95], the ground-state energy E can be found by minimizing the expected value of total Hamiltonian with respect to wave function:

$$E = \min_{\psi} \langle \psi | \hat{H} | \psi \rangle. \quad (2.2)$$

Here we take two steps for the minimization. For the first step, we minimize with respect to all wave functions give the same density $n(\vec{r})$:

$$E = \min_{\psi \rightarrow n} \langle \psi | \hat{T} + \hat{V}_{ee} | \psi \rangle + \int d\vec{r}^3 v(\vec{r}) n(\vec{r}). \quad (2.3)$$

Then with the resulting wave function ψ_n^{min} that yields minimum E and associate with density $n(\vec{r})$, we can construct universal functional:

$$\min_{\psi \rightarrow n} \langle \psi | \hat{T} + \hat{V}_{ee} | \psi \rangle = \langle \psi_n^{min} | \hat{T} + \hat{V}_{ee} | \psi_n^{min} \rangle = F[n(\vec{r})] \quad (2.4)$$

As seen in this equation, a functional, $F[n(\vec{r})]$, is a function of a function. For the second step, we minimized with respect to all densities $n(\vec{r})$:

$$E = \min_n \left\{ F[n(\vec{r})] + \int d\vec{r}^3 v(\vec{r}) n(\vec{r}) \right\}, \quad (2.5)$$

where $v(\vec{r})$ is kept fix during minimization. The resulting density is the ground-state density that gives lowest ground state energy. This is known as density variational principle, also the main idea of the Hohenberg-Kohn theorems. For the completeness, the theorems are present in the following:

Theorem 1 *The external potential, $V_{ext}(\vec{r})$, of any system of interacting particles is uniquely determined (up to a constant) by the particle density, $n_0(\vec{r})$, of the ground state.*

Theorem 2 *The ground state energy of a system with an external potential $V_{ext}(\vec{r})$ is given by the minimum value of the energy functional $E_{HK}[n]$ and the density for which this minimum is reached corresponds with the ground state density $n_0(\vec{r})$.*

Now, the main problem is to define the approximated expression of $F[n(\vec{r})]$. Kohn-Sham equation is a elegant way to do this. It aims to construct a non-interacting system, where kinetic energy can be calculated exactly, and add local external potential $V_{KS}(\vec{r})$. The $F[n]$ decomposed into following and define $E_{XC}[n]$ as exchange-correlation (XC) energy:

$$F[n] = T_s[n] + E_H[n] + E_{XC}[n], \quad (2.6)$$

where $T_s[n]$ is the non-interacting kinetic energy functional, and $E_H[n]$ is the Hartree energy functional:

$$E_H[n] = \frac{1}{2} \int d^3r \int d^3r' \frac{n(\vec{r})n(\vec{r}')}{|\vec{r} - \vec{r}'|}. \quad (2.7)$$

Apart from the last term, $E_{XC}[n]$, everything else can be exactly calculated for non-interacting system for given density. By imposing a normalisation constraint on the electron density, $\int n(\vec{r})d\vec{r} = N$, we have

$$\frac{\delta F[n]}{\delta n(\vec{r})} = -v(\vec{r}). \quad (2.8)$$

Therefore, the effective local potential, $V_{KS}(\vec{r})$, will be

$$V_{KS}(\vec{r}) = v(\vec{r}) + \frac{\delta E_H[n]}{\delta n(\vec{r})} + \frac{\delta E_{XC}[n]}{\delta n(\vec{r})}, \quad (2.9)$$

and the Kohn-Sham equation reads

$$\left[-\frac{1}{2}\nabla_i^2 + v(\vec{r}) + \frac{\delta E_H[n]}{\delta n(\vec{r})} + \frac{\delta E_{XC}[n]}{\delta n(\vec{r})} \right] \psi_\alpha(\vec{r}\sigma) = \epsilon_\alpha \psi_\alpha(\vec{r}\sigma), \quad (2.10)$$

and ground-state density is

$$n(\vec{r}) = \sum_{\alpha}^{\text{occ.}} \sum_{\sigma} |\psi_\alpha(\vec{r}\sigma)|^2. \quad (2.11)$$

This can be solved self-consistently. An initial guess on the density $n(\vec{r})$ determines the effective potential $V_{KS}(\vec{r})$, from Equation 2.10 wave functions $\psi_\alpha(\vec{r}\sigma)$ can be calculated, which will give a new density through Equation 2.11. This procedure is repeated until self-consistency is reached.

2.1.2 Exchange-correlation functional

The XC energy functional needs to be approximated. The choice of this directly influences the accuracy of the results. This is because, although it is often a small fraction of the total energy, its contribution to the chemical bonding and the formation energy is relatively important. The generalized gradient approximation (GGA) has become popular in solid state calculations. It

is a further upgrade of its previous version, the local density approximation (LDA). The LDA has the following form:

$$E_{XC}^{LDA}[n] = \int n(\vec{r})\epsilon_{XC}[n(\vec{r})]d\vec{r}. \quad (2.12)$$

$\epsilon_{XC}[n(\vec{r})]$ is the XC energy for homogeneous electron gas having density of n , and it is usually taken from quantum Monte Carlo calculations. Whereas the GGA further includes the derivative of density, $\nabla n(\vec{r})$, as an argument for ϵ_{XC} , thus it reads

$$E_{XC}^{GGA}[n] = \int \epsilon_{XC}[n(\vec{r}), \nabla n(\vec{r})]d\vec{r}. \quad (2.13)$$

Contrast to LDA, there is no unique input for $\epsilon_{XC}(n(\vec{r}), \nabla n(\vec{r}))$. Different constructions for GGA usually named with the corresponding authors, e.g. PW91-GGA stands for Perdew and Wang's GGA construction in 1991[96, 97] and PBE-GGA stands for Perdew, Burke, and Ernzerhof [98]'s construction. They are the most popular GGA approximations for solid state systems.

Jacob's ladder

Jacob's ladder is a ladder connecting earth and heaven that biblical Patriarch Jacob dreamed about. Professor John P. Perdew, who is known for profound contribution to DFT and XC functionals, used it analogously to describe the hierarchy of density functional approximations in terms of their accuracies, see Fig. 2.2.

Each rung is a level of approximation constructed with different formalisms. From LDA and GGA as mentioned to meta-GGA which includes the Kohn-Sham kinetic energy density. Next higher in the ladder is the hybrid functionals which incorporates a part of exact exchange from Hartree-Fock (HF) theory. For example, the PBE0 functional[100] has the following definition:

$$E_{XC}^{PBE0} = \frac{1}{4}E_X^{HF} + \frac{3}{4}E_X^{PBE} + E_C^{PBE}, \quad (2.14)$$

and the HSE06 (Heyd-Scuseria-Ernzerhof)[101] take into account the screen Coulomb potential for the exact part:

$$E_{XC}^{HSE} = \beta E_X^{HF,SR}(\omega) + (1 - \beta)E_X^{PBE,SR}(\omega) + E_X^{PBE,LR}(\omega) + E_C^{PBE}, \quad (2.15)$$

where β is the mixing parameter and ω is the parameter to control the screening range which defines the short-range, SR, and long-range, LR, parts. The values of $\beta = 1/4$ and $\omega =$

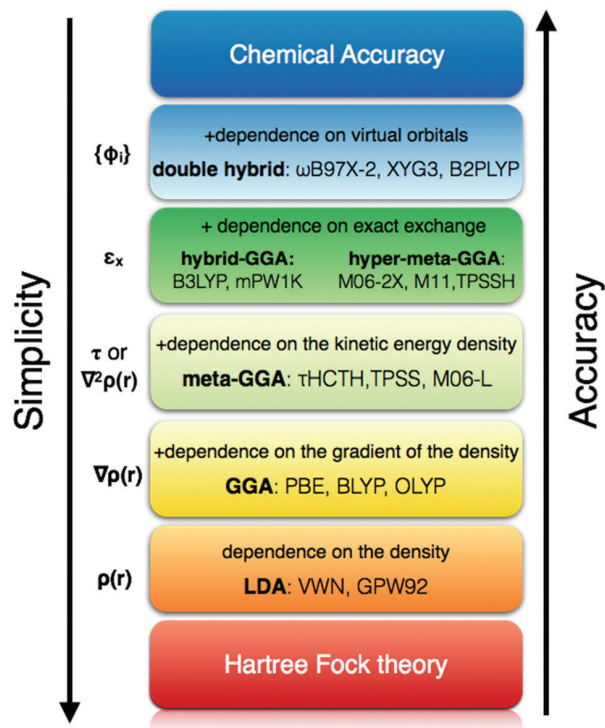


Fig. 2.2 Jacob's ladder for DFT approximations. Image source: [99].

- 1 0.2 corresponding to HSE06 functional which gives accurate band gaps and lattice constants,
- 2 see the Mean absolute error (MAE) of different functionals in Fig. 2.3.

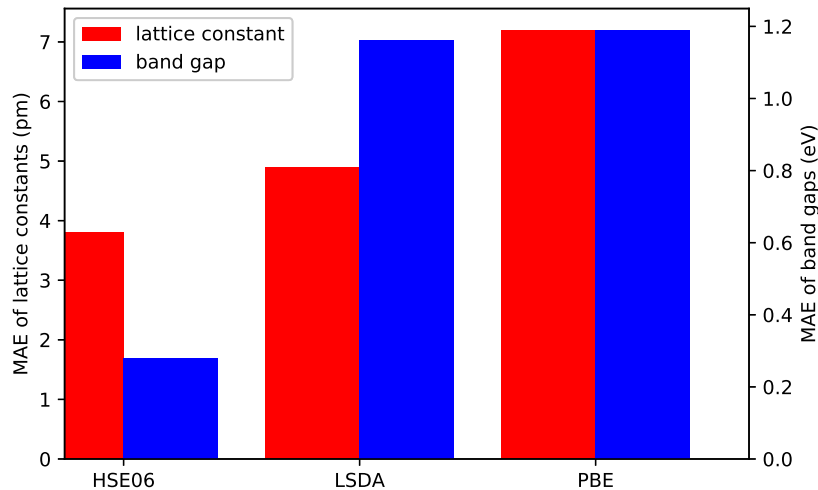


Fig. 2.3 MAE of the equilibrium lattice constants and band gaps of different functionals on SC40 solid test set. Data source: [102].

2.2 Implementation

25

The highest ranked functionals are the double hybrid which includes the unoccupied orbitals as well, e.g. Random Phase Approximation[103].

Band gap problem

As shown in Fig. 2.3, band gap estimation in LDA and GGA is quite poor. This can be attributed to the highly non-analytical and non-local behaviours of the XC energy functional. In other words, it means the energy increase by adding an extra electron in the extended system is of the order of 1 eV, even though, it is an infinitesimal density change. Let's look at the definition of the band gap E_g :

$$E_g = I - A = \epsilon_{N+1}^{KS,HOMO} - \epsilon_N^{KS,HOMO}, \quad (2.16)$$

where I is the ionization energy, the energy change by removing one valence electron; A is the electron affinity, the energy change by adding one electron to a neutral system; ϵ_N^{KS} Kohn-Sham orbital energy for N -electron system, and *HOMO* stand for the highest occupied molecular orbital; The *LUMO* below stands for the lowest unoccupied molecular orbital. For a non-interacting Kohn-Sham system, E_g^{KS} can be calculated as following:

$$E_g^{KS} = \epsilon_N^{KS,LUMO} - \epsilon_N^{KS,HOMO}. \quad (2.17)$$

This leads to

$$E_g = E_g^{KS} + \Delta_{XC}, \quad (2.18)$$

where Δ_{XC} is the orbital shift caused by adding an extra electron: $\epsilon_{N+1}^{KS,HOMO} - \epsilon_N^{KS,LUMO}$.

The Δ_{XC} exclusively depends on the non-analyticity of XC potential $\frac{\delta E_{XC}[n]}{\delta n(\vec{r})}$, since the Hartree potential explicitly depends on the density. If the XC energy functional were analytic, the infinitesimal density variation would not introduce large potential change, hence Δ_{XC} is small or equals to zero, and $E_g \approx E_g^{KS}$. The band gap accuracy when compared with experiment would be only limited inherently by different functionals. However, non-zero Δ_{XC} has been concluded on many materials and it is responsible for 80% of the LDA band gap error[105].

2.2 Implementation

The implementations of the theory in the last section are crucial and not always straightforward. Many of the quantities are represented with technically easy-implemented functions,

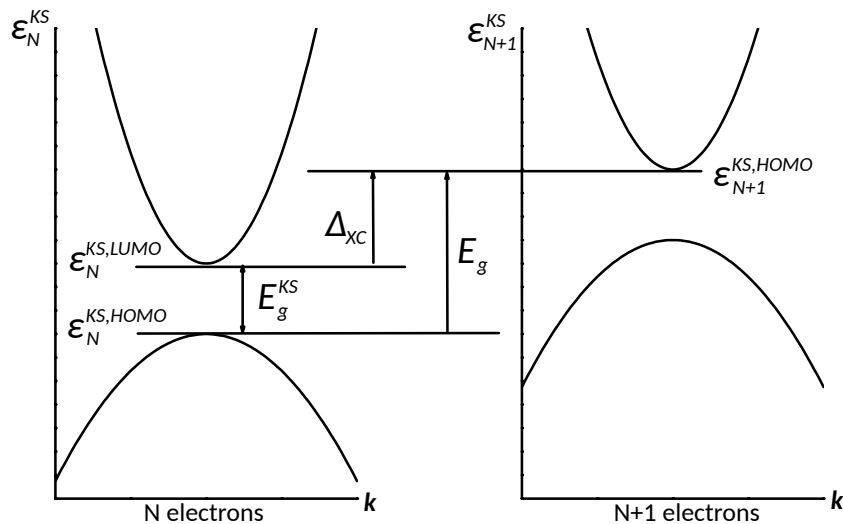


Fig. 2.4 Schematic illustration of the relation between E_g and E_g^{KS} . Image adapted from: [104].

- ¹ and they have to be finite in size or quantity. Question rises on how much would be enough?
- ² This is equivalent to the convergence of those in computation term. Here we review two of
- ³ the most important convergence parameters: \mathbf{k} points and cut-off energy of the basis set.

⁴ **k points**

- ⁵ According to the Bloch's theorem, the solution of Schrödinger equation for a periodic system,
- ⁶ e.g. crystal will well-defined unit cell, can be expressed through the following:

⁷
$$\phi_{\mathbf{k}}(\mathbf{r}) = e^{i\mathbf{k}\cdot\mathbf{r}} u_{\mathbf{k}}(\mathbf{r}), \quad (2.19)$$

⁸ where ϕ is the wave function, u is a function having same periodicity as the crystal. The
⁹ space of vector \mathbf{r} and \mathbf{k} are called real and reciprocal space (\mathbf{k} space), respectively. Particularly,
¹⁰ each point in the \mathbf{k} space associates with an unique \mathbf{k} vector and is usually called a \mathbf{k} point.
¹¹ Making use of the symmetry of the system, all inequivalent \mathbf{k} points reside inside a finite sub-
¹² space of \mathbf{k} space, called the first Brillouin zone (FBZ). Quantity evaluations are mostly done
¹³ through the integration of wave functions, or other functions have \mathbf{k} dependence, over the
¹⁴ FBZ. This integration has to be done numerically since explicit relation of ϕ and \mathbf{k} is unknown.
¹⁵ In practice, the FBZ is discretized into a grid defined by the mesh of the \mathbf{k} -points. This mesh
¹⁶ has to be large for accurate sampling of FBZ yet it should be small for less computational time
¹⁷ and resource. This is one of the convergence test need to be done for reliable results. Usu-
¹⁸ ally, metals needs more \mathbf{k} -points than semiconductors. This is because the highest occupied
¹⁹ valence band is crossed with Fermi energy in metals, hence the integration for all occupied

states is done for a discontinuous function that excludes unoccupied states. Whereas for a semiconductor or insulator, the highest occupied valence band is completely occupied, therefore it is a continuous function. Smearing is one of the ways to make discontinuous function in metal continuous by smearing out the edge using a smearing function, such as Fermi-Dirac function. The range of smearing has to compromise between the computation efficiency and correctness: Too large will give wrong integration results on the total energy, while too small become useless and again needs more k-points.

basis set, cut-off energy

Now let us look back at [Equation 2.19](#), we can identify $e^{i\mathbf{k}\cdot\mathbf{r}}$ as a plane wave. $u_{\mathbf{k}}(\mathbf{r})$ is periodic in space and it can be expanded in terms of a set of plane waves as well:

$$u_{\mathbf{k}}(\mathbf{r}) = \sum_{\mathbf{G}} c_{\mathbf{G}} e^{i\mathbf{G}\cdot\mathbf{r}}, \quad (2.20)$$

where $c_{\mathbf{G}}$ is the coefficient determines the magnitude of the plane wave $e^{i\mathbf{G}\cdot\mathbf{r}}$. [Equation 2.19](#) can now exclusively represent with plane waves:

$$\phi_{\mathbf{k}}(\mathbf{r}) = \sum_{\mathbf{G}} c_{\mathbf{k}+\mathbf{G}} e^{i\mathbf{k}+\mathbf{G}\cdot\mathbf{r}}. \quad (2.21)$$

The summation in above equation can not and not necessary to go to infinite to give accuracy results. The truncation usually done for the kinetic energy of the ϕ :

$$E = \frac{1}{2} |\mathbf{k} + \mathbf{G}|^2. \quad (2.22)$$

The maximum kinetic energy, E_{cut} , associates with a \mathbf{G} vector to limit the summations. Here we arrive at another convergence parameter plane wave cut-off energy. Similar to \mathbf{k} points, it has to be large enough for the convergence of the total energy, sometimes further requires that for the phonon frequency, is reached in an acceptable precision range. While too large will only cost more computational resources without additional benefits.

pseudopotentials

Considering the chemically inertness of the core electrons and their highly oscillating wave functions, their impact on valence electrons and other nuclei generally approximated by pseudopotentials to have a optimal computational efficiency. It is a smooth function has the ability to reconstruct the original core electron properties. In practice, a pseudopotential is constructed for one isolated atom of one element. While being used in complex multi-elements

1 system, the transferability of the pseudopotential is the key factor determine how well they
2 will perform. Ultrasoft [106] and projected augmented wave [107, 108] are two types of the
3 most popular pseudopotentials-based methods used in materials simulations. They are well-
4 balanced between the accuracy and the computational cost.

5 **2.2.1 Software Packages**

6 There are more than 70 different software packages capable of performing density functional
7 theory calculations according to Wikipedia[109]. They mainly differ in whether they include
8 pseudopotentials and which type, what type of basis set is used to the wave function expan-
9 sion, in which programming language it is written and is it free or commercial etc.. Lejaeghere
10 et al. [110] have compared 40 different implementations and their accuracy by comparing
11 their results to a highly accurate all-electron method. They concluded, all codes or methods
12 yield generally consistent results. The accuracy of the codes which were developed in recent
13 years is higher than the order ones. The Vienna *Ab initio* Simulation Package (VASP) [111, 112]
14 with its projected augmented wave method is one of the most accurate codes concluded from
15 this study. Its well-optimized performance on supercomputers gives good results in less time
16 as compared with the others. This code will be used as the main tool for all the calculations
17 done in this thesis.

Chapter 3

General physical properties 2D materials

In this thesis, the properties of materials are virtually divided into preliminary and advanced categories. In this chapter, we will focus on the preliminary properties of 2D materials, namely structural, electronic, vibrational and mechanical properties. These properties are considered as test calculations and knowledge which the advanced properties in the next chapter are closely related to. They are composed of both my original calculations and results from literatures. An emphasis will be made on the characteristic properties of 2D materials.

3.1 Structural properties

3.1.1 Layer structure

As has seen in the [chapter 1 Introduction](#), layered materials have a closest relationship with 2D materials. The strong anisotropic structure in the former results in the layer concept. This anisotropic nature attributes to the weak interlayer bonding and the strong intralayer bonding. The van der Waals interaction (vdWs)[113] is the main type of this weak bonding. vdWs is the attraction and repulsion between atoms or molecules entities caused by dipole-dipole, dipole-induced dipole and instantaneous induced dipole-induced dipole forces. The definition is sometimes extended to include other weak forces between molecules as well. For the 2D materials, vdWs interaction become important as the number of layers becomes larger than one: few-layer materials with typical number of layers less than ten. They also belong to the 2D materials family since the thickness of the materials still small such that quantum confinements still play role. As in its layered bulk part, a few-layer system is stacked of monolayers that hold together through vdWs. When no other bonding types are presented, interlayer vdWs determines all the change brought by going above single layer and its impact on the electronic structure will be significant. For example, as going from monolayer to bilayer,

- ¹ the linear dispersion relation of energy E and momentum k evolves into parabolic-like spec-
² trum[114, 115].

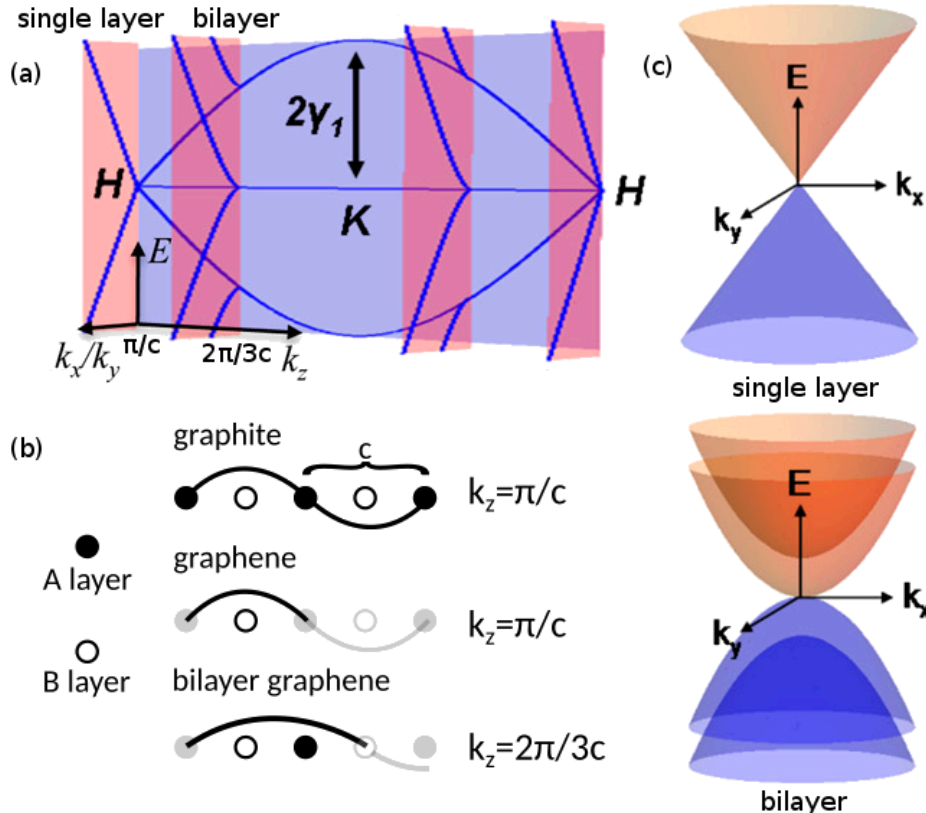


Fig. 3.1 Energy-momentum dispersion relation of single layer and bilayer graphene as plane intersections of 3D graphite dispersion. Image adapted from: [115].

- ³ In Fig. 3.1 (a), the dispersion relation in graphite along the z direction, that is the HKH line
⁴ in the Brillouin zone, is shown in blue plane. This direction is perpendicular to the graphite
⁵ layers. Because of the interlayer interaction and quantum confinements, in few-layer system,
⁶ the finite thickness limits the number of wave vectors that standing waves can take. There-
⁷ fore, if only the intralayer and interlayer interactions between nearest neighbour atoms were
⁸ considered, the dispersion relations in few-layer systems could be considered as the disper-
⁹ sions on the corss-section of red planes that cut the graphite Brillouin zone, see Fig. 3.1 (a).
¹⁰ These planes are perpendicular to the z direction and intersect with the HKH line at possible
¹¹ points. This is called the zone-folding of dispersion relations[116]. These points are illustrated
¹² in Fig. 3.1 (b). Under the condition that quantum confinements at few-layer system require
¹³ the wave functions vanish at the imaginary layer outside the surface of the system, the sys-
¹⁴ tems will have well-defined wave vectors. Then, the dispersion relations will be on the plane
¹⁵ intersects at $k_z = \pi/c$ and at $k_z = 2(\pi/3c)$ for graphene and bilayer graphene, respectively.

Having the knowledge of 3D band structure of graphite, we can approximate the dispersion of few-layer systems in this way. As a result, as shown in red plane in Fig. 3.1 (a) and their 3D version in Fig. 3.1 (c), graphene has linear dispersion relations and bilayer graphene has parabolic-like two dispersion bands. Moreover, the bilayer structure will never pass through the H point where graphene has passed and have linear dispersion relation. This is because of standing waves in bilayer will have a wave vector $k = 2(n\pi/3c)$, where n is a positive integer: 1, 2, ..., n . This will not equal to π/c for any number of n . More generally, systems with an even number of layers will not have linear dispersion; whereas systems with an odd number of layers always have linear dispersion relation. Further, if other interactions were considered, an overlap of bands those touch each other in (c) would happen[114]. This overlap increases with the number of layers. Eventually in graphite, maximum overlap is reached.

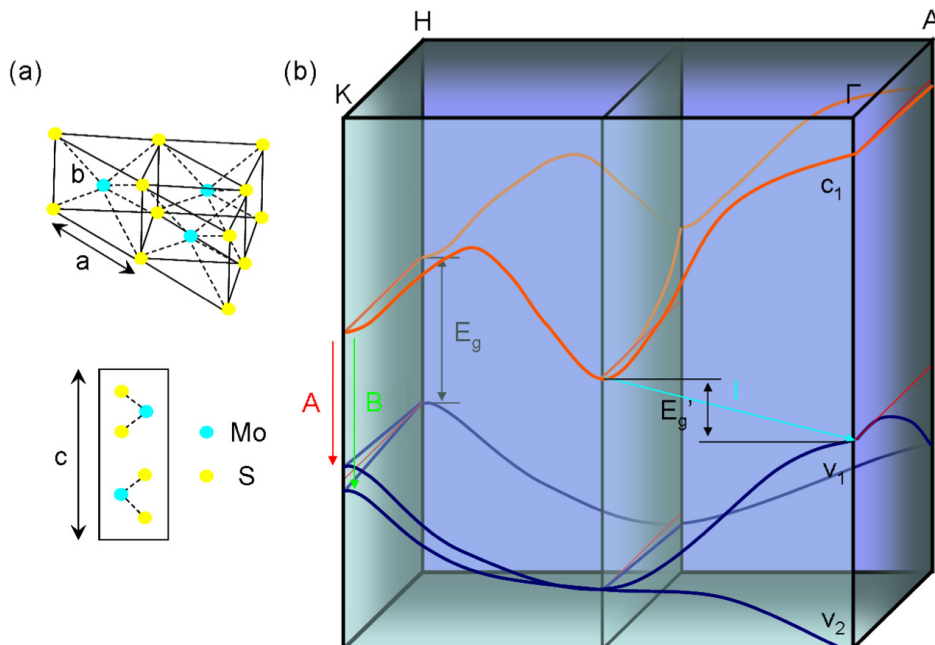


Fig. 3.2 Energy-momentum dispersion relation of single layer and bulk graphene as plane intersections of 3D graphite dispersion. Image adapted from: [117].

Another example of the importance of interlayer interaction in the few-layer 2D materials will be the MoS₂. As mentioned in the [chapter 1 Introduction](#), as going from bulk to monolayer, MoS₂ transforms from an indirect band gap to a direct one. Here again we can make use of zone-folding to approximate the band structure of monolayer from layered bulk one. The monolayer and the layered structure of 2H phase is shown in Fig. 3.2 (a). In (b) let us focus on the difference of dispersion relations on the planes parallel to the page passing through KΓ and HA lines (simply call them KΓ and HA planes below). Same as the graphite, 2H layered MoS₂ has two layers per unit cell. Therefore, according to the standing wave arguments that

we have used for graphene above, HA plane represents the monolayer. E_g and E_{lg} are the band gap of monolayer and layered bulk structures. Here not only the magnitude of band gap increased as going from bulk to monolayer, character of the band gap has changed as well. It is shown that this is due to the band edges change. Interlayer interactions widen top valence bands at Γ and bottom conduction band at the middle of ΓK line, which without interlayer interaction should be degenerated. Therefore, these two band edges become the ones those determine the band gap instead of band edges at K in the monolayer. Contrast to this, band edges at K are not effected too much by the interlayer interaction to make a difference. When we compare the difference between band edges of K and other two is, we could find out that the latter two have much larger contribution from p_z orbitals that give maximum interlayer orbital overlap hence interlayer interaction than d orbitals that dominant at K point.

3.1.2 sp hybridization

When atoms come together form bonds, the orientations of these bonds are decisive for the final structure. The sp hybridization is a good example of this. It can mainly exist in three different variants: sp, sp^2 and sp^3 , see Fig. 3.3. The hybridization index n in sp^n stands for the relative amount of p character in the hybridization. For example, sp^2 has 1/3 s character and 2/3 p character. Hybridized bonds tend to maximized their distance to reduce the energy raised by the repulsion of electrons. As shown in Fig. 3.3, this results in tetrahedral structure of diamond that made of sp^3 bonds, trigonal planar structure of graphite or graphene that made of sp^2 and linear structure of ethyne molecules that made of sp bonds. Coulson and Moffitt [118] generalized the relation of bond angle and n in the following way:

$$1 = -\sqrt{n_1 n_2} \cos\theta_{12}, \quad (3.1)$$

where θ_{12} is the bond angle between orbital 1 and 2. The bond angle can be measured in atomic simulations, yet we still need one more constrain to solve the equation for n if orbital 1 and 2 have different n . This constrain is that, in the case of carbon atom, the total fractions of all s hybridized orbitals should equal 1, while it should be 3 for the sum of the p fractions. Consequently, each bond from one atom can be assigned with a unique n . This formula is useful to determine the s and p composition of the bonds. For example, $\theta_{12} = 90^\circ$ gives $n \rightarrow \infty$, which means it is pure p orbital; $\theta_{12} = 120^\circ$ gives $n = 2$, that is a sp^2 bond. Generally, wider bond angle corresponds to large s contribution. Of course, this is more useful when the bond angle takes value other than those three types of hybridized bonds mentioned. Then we can use it to explain resulting geometrical structure.

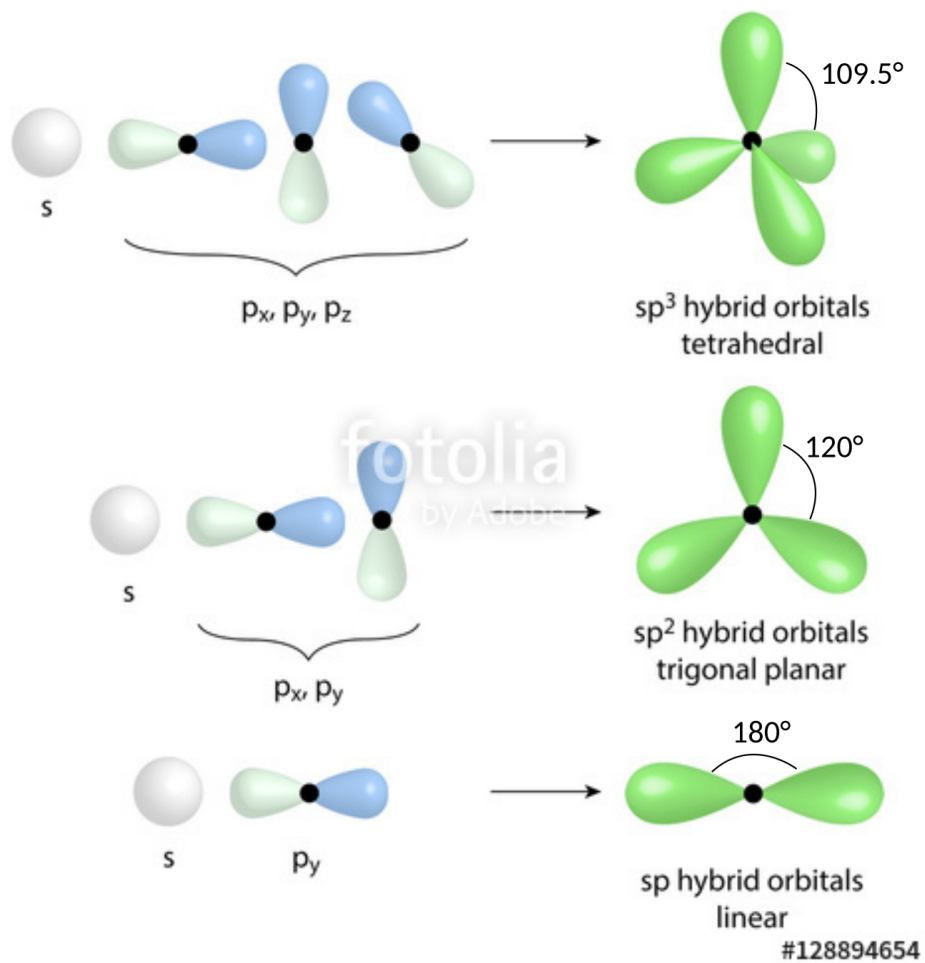


Fig. 3.3 Three types of sp hybridization. Image adapted from: [119].

¹ 3.2 Electronic properties

² Electronic properties is one of the first feature we usually like to know about the new mate-
³ rials. Not only it is because semiconductor and metal have different role in applications, but
⁴ also because the details of the electronic structure set the direction towards which further
⁵ exploration should be carried out. One example for this from my experience is that from mon-
⁶ itoring the electronic structure variations under a strain we had predicted how the mobility
⁷ of the carrier can be tuned. This will be discussed in the later chapter. Therefore, it is impor-
⁸ tant to understand this property of a new material to fully reveal its potentials. Electronic
⁹ properties usually characterized by band structure (BS) and density of states (DOS). These cal-
¹⁰ culations are standard calculations in first-principles codes where all consequent calculations
¹¹ start. After solving the Kohn-Sham equation with proper cut-off energy, k points etc., we will
¹² have all eigenenergy of each state identified with k point in the Brillouin zone and band index.
¹³ DOS is a count of the number of states at specific energy. BS is the plot of eigenenergy verse
¹⁴ the line in Brillouin zone that connects high symmetry k points. 2D material has vast variation
¹⁵ of electronic properties. From semimetallic graphene to semiconducting MoS₂ and to insu-
¹⁶ lating BN. We have already seen these in the introduction. The purpose of this section is to
¹⁷ point out some of the interesting electronic properties of some 2D materials. We will start
¹⁸ with a brief introduction to the electronic properties of graphene.

¹⁹ 3.2.1 Example: graphene

²⁰ As mentioned before, orbitals in graphene are sp² hybridized. Each one of this sp² orbitals,
²¹ coloured as green in Fig. 3.4, are composed from s, p_x and p_y orbitals. The p_z orbital is left
²² unchanged, coloured as yellow in the figure. One sp² hybridized orbital with another one
²³ from adjacent atom form strong σ bond, while p_z orbitals form π bonds. It may look like an
²⁴ alternative single and double bonds between atoms, actually according to the Clar's theory,
²⁵ the bond order, i.e. the number of chemical bonds between a pair of atoms, in graphene is
²⁶ 4/3 and it is uniform[120].

²⁷ Every atom has same local environment, however, adjacent atoms are not equivalent.
²⁸ They belong to different hexagonal sublattices A and B as indicated with blue and yellow
²⁹ colors in Fig. 3.5. a_1 and a_2 are the basis vectors in real space connecting equivalent sites. b_1
³⁰ and b_2 are the basis vectors in reciprocal space connecting equivalent k points. The hexagon
³¹ in the reciprocal space is the first Brillouin zone where all inequivalent k points are contained.
³² These kpoints associate with different parallel lines of atoms and thus also indicate differ-
³³ ent directions in the real space. The k wave vectors near the Γ point have longer wave length,
³⁴ while those at the boundary of the first Brillouin zone have a wave length that is two times the

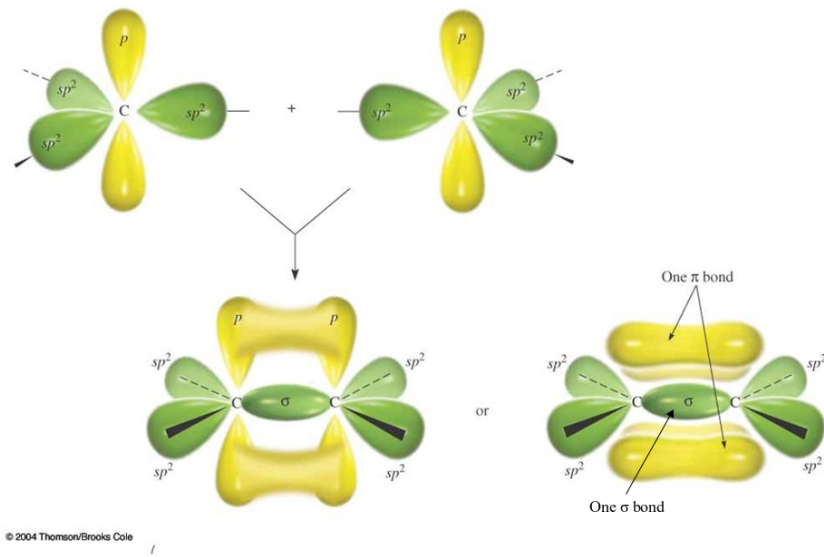


Fig. 3.4 The formation of $sp^2 \sigma$ and $p_z \pi$ double bond. Image source: [121].

unitcell dimension on that direction. For example, the most interesting k point for graphene is the K and K' points. These directions correspond to the a_1 and a_2 directions in real space. It is only at these k points in the Brillouin zone, the antibinding and bonding π band touch each other. Addition to this, as we have discussed in the introduction the Dirac cones will form around theses k points.

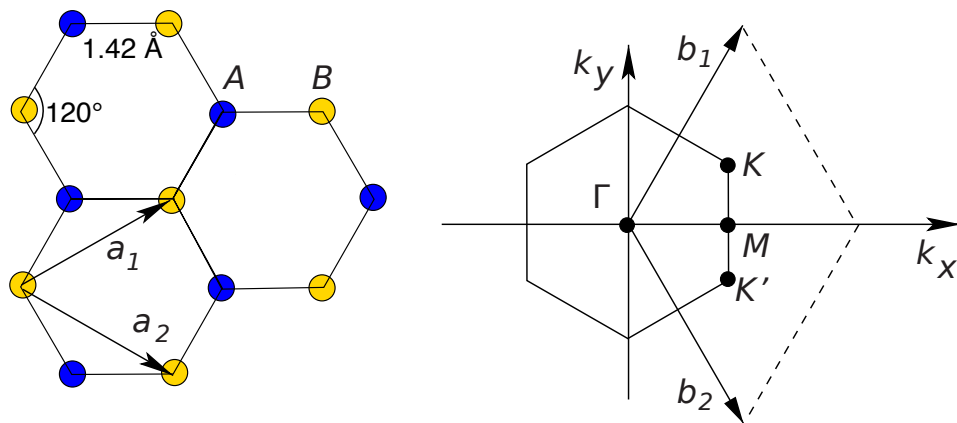


Fig. 3.5 Graphene lattice and its Brillouin zone. Image source: [14].

As compared to π bond, σ bond originate from strong overlap of sp^2 orbitals. The interaction is strong and the splitting of bonding and antibonding orbitals are large. Which makes the σ bonding orbitals deep in energy, or in other word, makes it strong and difficult to break. This feature contribute the most to the mechanical strength of graphene. On the other hand,

¹ p_z orbitals are less overlapped. This makes the π bond energy close to Fermi level, i.e. the
² highest occupied state. Therefore, they contribute the most to the electronic properties of
³ graphene.

⁴ 3.2.2 Dirac cone and symmetry

⁵ We have seen that graphene, silicene and germanene have an interesting electronic structure:
⁶ Dirac cone. We also have listed the consequences of having such feature: high mobility,
⁷ massless carrier etc.. In this section, we will discuss the symmetry condition for the existence
⁸ of Dirac cones. This knowledge is useful to find more materials of this type.

⁹ According to von Neumann-Wigner theorem, the space-time inversion symmetry is crucial
¹⁰ for the existence and protection of Dirac cones[122]. It is a combination of space inversion and
¹¹ time reversal symmetries. These two are equally important and has to act simultaneously for
¹² the possible formation of Dirac cones. More restrict condition that guarantee the existence of
¹³ Dirac cones has to deal with relations of hopping integrals[123, 124]. It is from the Liu, Wang,
¹⁴ and Li [124]'s study that it revealed the hexagonal lattice has the most favourable structure to
¹⁵ posses Dirac cones. The probability decreases as one goes from hexagonal to square lattice,
¹⁶ as shown in Fig. 3.6.

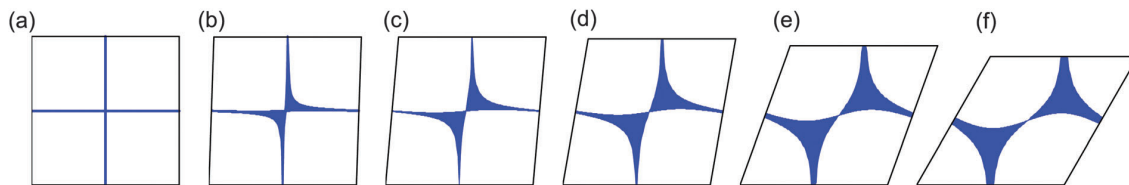


Fig. 3.6 Possible positions of second atom (blue area) to guarantee the existence of Dirac cones as going from (a) square lattice to (f) hexagonal lattice. The first atom is located at the corners of the unit cell. Image source: [124].

¹⁷ erpan: still need to write something about this section.

¹⁸ 3.2.3 Polar bond

¹⁹ 3.2.4 Accurate description from DFT

²⁰ 3.3 Vibrational properties

²¹ The force on a atom can be calculated from wave functions that are evaluated from DFT thanks
²² to the Hellmann-Feynman theorem. When searching for the equilibrium geometry of the ma-

terials, one basically trying different positions of atoms to find a geometry that minimized all the forces. This usually is the first thing to do for a new materials, since different codes, implementation and, more importantly, different functionals will give different results. Despite the fact that the difference is usually small, unrelaxed geometry will have residual forces on atoms. This is particularly important when vibrational properties are concerned. The way vibrational properties are characterized are through the energy (usually expressed in terms of frequency) verse vibrational wave vector dispersion relations. In crystal, All atoms have a equilibrium positions that consist with the lattice points. Atoms vibrate around their equilibrium positions. The vibrational modes are quantized into phonons. Each phonon represent a periodic, collective vibration with well-defined vibrational mode and wave vector. The forces (F) resort the atoms when they deviate from their equilibrium positions can be calculate from DFT either by introducing small displacement or from perturbation theory. Then, force constants, Φ , can be constructed by monitoring the forces change through displacements, u , of atoms in the following way:

$$\Phi_{i\alpha,j\beta} = \frac{\partial F_{j\beta}}{\partial u_{i\alpha}}, \quad (3.2)$$

where the i, j indices are the label for atoms, α, β are the Cartesian directions. The Fourier transformation of the force constants at wave vector \mathbf{q} is the dynamical matrix $D(\mathbf{q})$ that related to the frequency of the phonon through eigenvalue problem:

$$\omega^2(\mathbf{q}, n)\mathbf{e}(\mathbf{q}, n) = D(\mathbf{q})\mathbf{e}(\mathbf{q}, n), \quad (3.3)$$

where ω is the frequency of the phonon in mode n having a \mathbf{q} wave vector, and $\mathbf{e}(\mathbf{q}, n)$ is the eigenvector[125, 126]. These modes of phonons categorized into two main branches: acoustic and optical modes. Optical mode has differently charge polarized atoms vibrate with respect to each other and can interact with light, while acoustic mode all atoms in the unit cell move in phase. Further, considering the directions of the wave (\mathbf{e}) and vibration (\mathbf{q}), the modes subcategorized into transverse optical (TO) and transvers acoustic (TA): ($\mathbf{q} \perp \mathbf{e}$), longitudinal optical (LO) and longitudinal acoustic (LA) ($\mathbf{q} \parallel \mathbf{e}$). These modes are all in-plane vibrations for 2D materials. For such a case, another direction is also important, namely the \mathbf{c} lattice vector perpendicular to the 2D plane. Therefore, special modes exist: out-of-plane transverse optical (ZO) and out-of-plane transverse acoustic (ZA) ($\mathbf{q} \perp \mathbf{e}$ and $\mathbf{q} \parallel \mathbf{c}$). The total number of acoustic modes is three, that of optical modes is 3N-3.

¹ 3.3.1 Example: monolayer MoS₂

² Let us now take an example of layered bulk and monolayer MoS₂ to highlight some of the
³ important details of phonon dispersion relations. A mode comparison between bulk and
⁴ monolayer MoS₂ is presented in Fig. 3.7 (a). The reduction of dimensionality also reduce
⁵ the independent optical modes. Another characteristic feature of layered and 2D materials is
⁶ the quadratic ZA mode (flexural mode). It is usually linear in 3D bulk materials. The interlayer
⁷ interaction is weak in layered and absent in 2D materials make this mode soft. As can be seen
⁸ in Fig. 3.7 (b), phonon with longer wave length in ZA mode has smaller frequency or energy. It
⁹ means this mode is easier get excited at low temperature and forms ripples which have been
¹⁰ commonly observed in 2D materials.

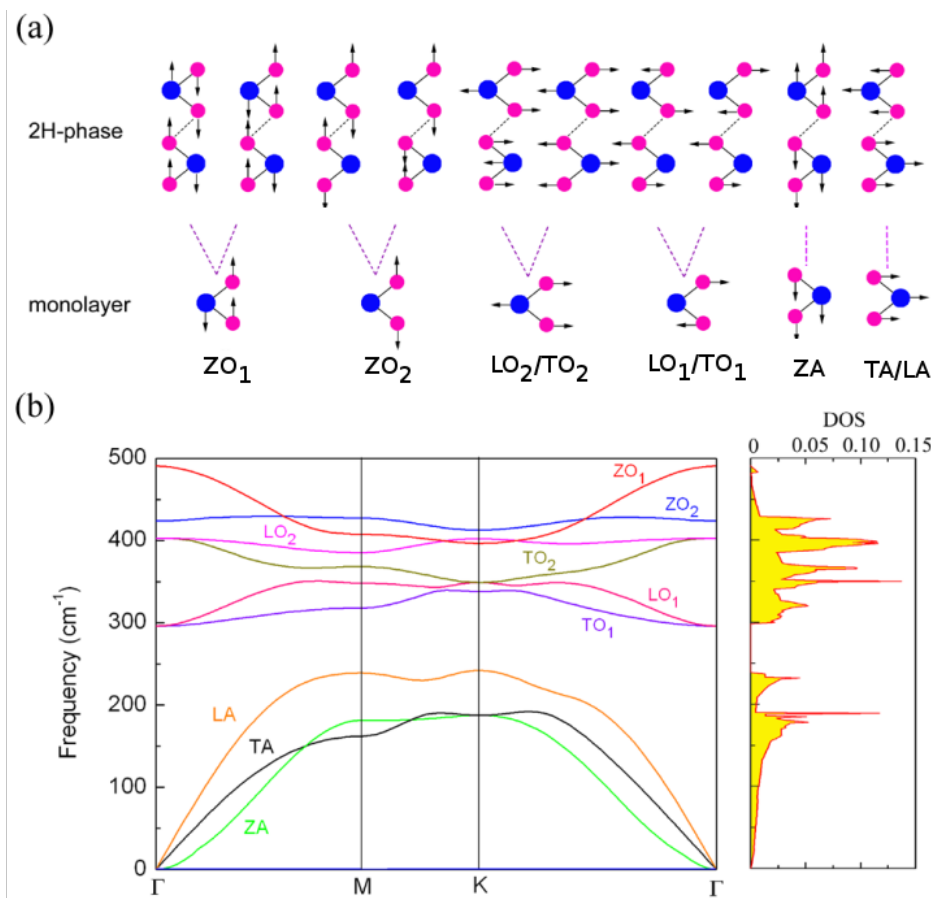


Fig. 3.7 (a) phonon modes of bulk (first row) and monolayer MoS₂ at Γ q point. (b) phonon dispersion and DOS of monolayer MoS₂. Image adapted from: [127].

3.3.2 Dynamic stability from phonon dispersion

One of the most important output of phonon dispersion is the dynamical stability of the structure. The instability of a structure usually captured by the presence of imaginary frequency in its phonon dispersions, see Fig. 3.8 for example.

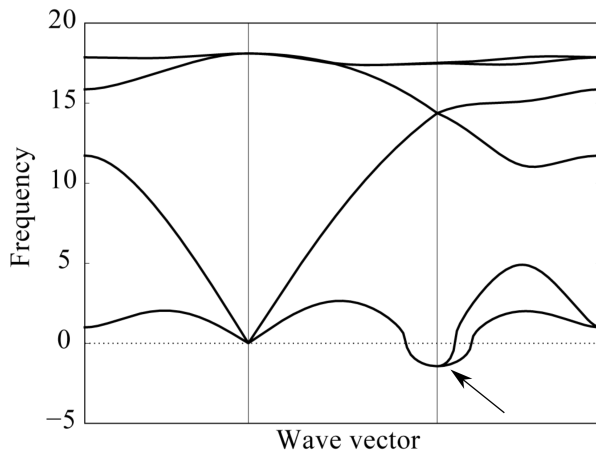


Fig. 3.8 Imaginary frequencies shown as negative frequencies in a phonon dispersion plot.

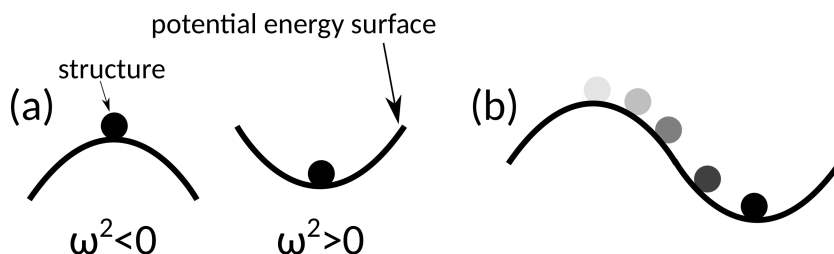


Fig. 3.9 (a) A structure at the convex (left) and concave (right) of the PES. (b) Searching for stable structure (phase transition).

Consider a relaxed structure that forces on all atoms are vanished. This could be on a convex or a concave of the potential energy surface (PES), see Fig. 3.9. Note that, in both situations the force are zero, which means both situations can happen when the structure is relaxed only following the force. In the case of PES convex, the dynamical matrix $D(\mathbf{q})$ will have negative components related to the square of frequency ω , hence imaginary frequency is the solution. Structure with imaginary frequency near Γ q point not necessarily means it is not stable. Since a large supercell consist of multiple of unit cell is typically used to do phonon calculations. It may happen the size of the supercell is not large enough to correctly describe long wavelength phonons. However, structure with imaginary frequency appears at other q points than Γ would imply a structure instability or structural phase transition is

¹ preferred. Nonetheless, with advanced technique in software[128], it is possible to modulate
² such structure based on the vibration mode which has imaginary frequency to find a lower
³ energy state and stabilize the structure, as illustrated in Fig. 3.9 (b).

⁴ 3.4 Mechanical properties

⁵ In chapter 1 Introduction, we have seen the stiffness and strength of some of the 2D materials.
⁶ They all belong to the mechanical properties of the materials. Force on atoms or the stress σ
⁷ on the unit cell under finite strain ϵ are the typical outputs from first-principles codes. Within
⁸ the elastic regime of stress-strain relation, they can be related through elastic constant C :
⁹ $\sigma = C\epsilon$, this is the Hook's law. C is a 6×6 matrix whose matrix elements has a form C_{ij} . The
¹⁰ elements measure the resistance of materials in i direction to a deformation in j direction,
¹¹ where i and j are the index of stress and strain tensors, respectively. Under the Voigt notations,
¹² the indices have the following correspondence: 1→ xx, 2→ yy, 3→ zz, 4→ yz, 5→ zx, 6→ xy.
¹³ In 2D hexagonal lattice symmetry, the Hook's law reads:

$$\begin{pmatrix} \sigma_1 \\ \sigma_2 \\ \sigma_6 \end{pmatrix} = \begin{pmatrix} C_{11} & C_{12} & 0 \\ C_{12} & C_{11} & 0 \\ 0 & 0 & (C_{11} - C_{12})/2 \end{pmatrix} \begin{pmatrix} \epsilon_1 \\ \epsilon_2 \\ \epsilon_6 \end{pmatrix}. \quad (3.4)$$

¹⁵ In this way, all elastic constants can be extract from stress-strain data from the first-principles■
¹⁶ calculations. However, it is more convenient to have one quantity to describe each aspect of
¹⁷ the mechanical properties of the materials. This is where Young's modulus Y , shear modulus
¹⁸ G and Poisson's ratio ν become useful. Following the previous notation, they defined as

$$Y_\alpha = \frac{1}{S_{\alpha\alpha}}, \quad \alpha = 1, 2, 3. \quad (3.5)$$

$$\nu_{\alpha\beta} = -Y_\beta S_{\alpha\beta}, \quad \alpha, \beta = 1, 2, 3 \quad (\alpha \neq \beta). \quad (3.6)$$

$$G_{\gamma\gamma} = \frac{1}{S_{\gamma\gamma}}, \quad \gamma = 4, 5, 6, \quad (3.7)$$

²² where $S = C^{-1}$ is the compliance matrix [e.g. 129]. Young's and shear modulus give
²³ the stiffness of the materials to stretching and shearing deformation on particular direction.
²⁴ Whereas Poisson's ratio gives the ratio of the transverse to the axial strain, represents how
²⁵ easy it is to change the shape of the material with respect to the volume. Liquid and rub-
²⁶ ber have a Poisson's ratio close to 0.5, which is the theoretical upper limit of this quantity.

3.4 Mechanical properties**41**

Breaking strength/strain is a measure of load limit that the material can sustain, and it is characterized how strong a material is. This quantity is usually obtained by continuously deform the materials until it break where the maximum stress/strain gives the corresponding limits.

1
2
3**3.4.1 Elastic and engineering constants**

4

3.4.2 Mechanical stability: Born stability criteria

5

Draft - v1.0

Tuesday 30th May, 2017 – 17:32

Draft - v1.0

Tuesday 30th May, 2017 – 17:32

¹ Chapter 4

² Results of Physical Properties Calculations ³ in Novel 2D materials

⁴ 4.1 Thermal properties

⁵ 4.1.1 Thermal expansion and anharmonic oscillations

⁶ 4.1.2 Quasi-harmonic approximation

⁷ 4.1.3 Helmholtz free energy and specific heat

⁸ 4.2 Piezoelectric properties

⁹ 4.2.1 Piezoelectric constants

¹⁰ 4.2.2 Importance of internal relaxation

¹¹ 4.3 Carrier transport properties

¹² 4.3.1 Carrier mobility

¹³ 4.3.2 Deformation potential theory: non-polar materials

¹⁴ 4.3.3 Deformation potential theory: polar materials

¹⁵ 4.4 Magnetic properties

¹⁶ 4.4.1 Magnetic ordering

¹⁷ Stoner criterion of ferromagnetism

¹⁸ 4.5 Battery related properties

Draft - v1.0

Tuesday 30th May, 2017 – 17:32

¹ Chapter 5

² Results of Physical Properties Modification ³ in Novel 2D materials

⁴ 5.1 Number of layers and types of stackings

⁵ 5.1.1 Electronic properties

⁶ 5.1.2 Vibrational properties

⁷ 5.2 Mechanical strain

⁸ 5.2.1 Carrier mobility

⁹ 5.2.2 Magnetic properties

¹⁰ 5.3 Adatom adsorption

¹¹ 5.3.1 Electronic properties

¹² 5.4 Heterostructures

¹³ 5.4.1 Electronic properties

¹⁴ 5.4.2 Li diffusion

¹⁵ 5.5 Defect induction

¹⁶ 5.5.1 Structural properties

¹⁷ 5.5.2 Electronic properties

¹⁸ 5.5.3 Magnetic properties

Chapter 6

1

Conclusions

2

Draft - v1.0

Tuesday 30th May, 2017 – 17:32

References

- [1] K. S. Novoselov et al. "Electric Field Effect in Atomically Thin Carbon Films". In: *Science* 306.5696 (2004), pp. 666–669. DOI: [10.1126/science.1102896](https://doi.org/10.1126/science.1102896) (cit. on p. 1). 1
- [2] K. S. Novoselov et al. "Two-dimensional atomic crystals". In: *Proceedings of the National Academy of Sciences of the United States of America* 102.30 (2005), pp. 10451–10453. DOI: [10.1073/pnas.0502848102](https://doi.org/10.1073/pnas.0502848102) (cit. on pp. 1, 14). 2
- [3] A. K. Geim and K. S. Novoselov. "The rise of graphene". In: *Nat. Mater.* 6.3 (Mar. 2007), pp. 183–191. DOI: [10.1038/nmat1849](https://doi.org/10.1038/nmat1849) (cit. on pp. 1, 5). 3
- [4] The Royal Swedish Academy of Sciences. *The Nobel Prize in Physics 2010 - Information for the public*. 2010. URL: https://www.nobelprize.org/nobel_prizes/physics/laureates/2010/popular-physicsprize2010.pdf (visited on 04/14/2017) (cit. on p. 4). 4
- [5] H. Petroski. *The Pencil: A History of Design and Circumstance*. Knopf, 1990 (cit. on p. 3). 5
- [6] A. Krishnan et al. "Graphitic cones and the nucleation of curved carbon surfaces". In: *Nature* 388.6641 (July 1997), pp. 451–454. DOI: [10.1038/41284](https://doi.org/10.1038/41284) (cit. on pp. 3, 5). 6
- [7] Y. Ohashi et al. "Size Effect in the In-plane Electrical Resistivity of Very Thin Graphite Crystals". In: *TANSO* 1997.180 (1997), pp. 235–238. DOI: [10.7209/tanso.1997.235](https://doi.org/10.7209/tanso.1997.235) (cit. on pp. 3, 5). 7
- [8] M. S. Dresselhaus and G. Dresselhaus. "Intercalation compounds of graphite". In: *Advances in Physics* 51.1 (2002), pp. 1–186. DOI: [10.1080/00018730110113644](https://doi.org/10.1080/00018730110113644) (cit. on p. 3). 8
- [9] H. Shioyama. "Cleavage of graphite to graphene". In: *Journal of Materials Science Letters* 20.6 (2001), pp. 499–500. DOI: [10.1023/A:1010907928709](https://doi.org/10.1023/A:1010907928709) (cit. on p. 3). 9
- [10] R. Peierls. "Quelques propriétés typiques des corps solides". fre. In: *Annales de l'institut Henri Poincaré* 5.3 (1935), pp. 177–222 (cit. on p. 3). 10
- [11] Lev Davidovich Landau. "On the theory of phase transitions. I." In: *Phys. Z. Sowjet.* 11 (1937), p. 26 (cit. on p. 3). 11
- [12] N. D. Mermin. "Crystalline Order in Two Dimensions". In: *Phys. Rev.* 176 (1 Dec. 1968), pp. 250–254. DOI: [10.1103/PhysRev.176.250](https://doi.org/10.1103/PhysRev.176.250) (cit. on p. 3). 12
- [13] P. R. Wallace. "The Band Theory of Graphite". In: *Phys. Rev.* 71 (9 May 1947), pp. 622–634. DOI: [10.1103/PhysRev.71.622](https://doi.org/10.1103/PhysRev.71.622) (cit. on pp. 3, 5). 13
- [14] a. H. Castro Neto et al. "The electronic properties of graphene". In: *Rev. Mod. Phys.* 81.1 (Jan. 2009), pp. 109–162. DOI: [10.1103/RevModPhys.81.109](https://doi.org/10.1103/RevModPhys.81.109) (cit. on pp. 3, 35). 14
- [15] H. W. Kroto et al. "C₆₀: Buckminsterfullerene". In: *Nature* 318.6042 (Nov. 1985), pp. 162–163. DOI: [10.1038/318162a0](https://doi.org/10.1038/318162a0) (cit. on p. 3). 15

- 1 [16] W. Krätschmer et al. "Solid C₆₀: a new form of carbon". In: *Nature* 347.6291 (Sept.
2 1990), pp. 354–358. DOI: [10.1038/347354a0](https://doi.org/10.1038/347354a0) (cit. on p. 3).
- 3 [17] Sumio Iijima and Toshinari Ichihashi. "Single-shell carbon nanotubes of 1-nm diameter". In: *Nature* 363.6430 (June 1993), pp. 603–605. DOI: [10.1038/363603a0](https://doi.org/10.1038/363603a0) (cit. on
4 p. 3).
- 6 [18] Ray H. Baughman, Anvar A. Zakhidov, and Walt A. de Heer. "Carbon Nanotubes—the
7 Route Toward Applications". In: *Science* 297.5582 (2002), pp. 787–792. DOI: [10.1126/science.1060928](https://doi.org/10.1126/science.1060928) (cit. on p. 5).
- 9 [19] K. S. Novoselov et al. "Two-dimensional gas of massless Dirac fermions in graphene". In:
10 *Nature* 438.7065 (Nov. 2005), pp. 197–200. DOI: [10.1038/nature04233](https://doi.org/10.1038/nature04233) (cit. on
11 p. 5).
- 12 [20] M. I. Katsnelson, K. S. Novoselov, and A. K. Geim. "Chiral tunnelling and the Klein para-
13 dox in graphene". In: *Nat Phys* 2.9 (Sept. 2006), pp. 620–625. DOI: [10.1038/nphys384](https://doi.org/10.1038/nphys384)
14 (cit. on p. 5).
- 15 [21] K. S. Novoselov et al. "Room-Temperature Quantum Hall Effect in Graphene". In: *Sci-
16 ence* 315.5817 (2007), pp. 1379–1379. DOI: [10.1126/science.1137201](https://doi.org/10.1126/science.1137201) (cit. on p. 5).
- 17 [22] J Güttinger et al. "Transport through graphene quantum dots". In: *Reports on Progress
18 in Physics* 75.12 (2012), p. 126502 (cit. on p. 6).
- 19 [23] Changgu Lee et al. "Measurement of the Elastic Properties and Intrinsic Strength of
20 Monolayer Graphene". In: *Science* 321.5887 (2008), pp. 385–388. DOI: [10.1126/science.1157996](https://doi.org/10.1126/science.1157996) (cit. on p. 6).
- 22 [24] K.I. Bolotin et al. "Ultrahigh electron mobility in suspended graphene". In: *Solid State
23 Communications* 146.9-10 (2008), pp. 351–355. DOI: [10.1016/j.ssc.2008.02.024](https://doi.org/10.1016/j.ssc.2008.02.024) (cit.
24 on p. 6).
- 25 [25] K. I. Bolotin et al. "Temperature-Dependent Transport in Suspended Graphene". In:
26 *Phys. Rev. Lett.* 101 (9 Aug. 2008), p. 096802. DOI: [10.1103/PhysRevLett.101.096802](https://doi.org/10.1103/PhysRevLett.101.096802)
27 (cit. on p. 6).
- 28 [26] Alexander A Balandin et al. "Superior thermal conductivity of single-layer graphene". In:
29 *Nano letters* 8.3 (2008), pp. 902–907 (cit. on p. 6).
- 30 [27] Lijie Ci et al. "Atomic layers of hybridized boron nitride and graphene domains". In:
31 *Nature Materials* 9.5 (Feb. 2010), pp. 430–435. DOI: [10.1038/nmat2711](https://doi.org/10.1038/nmat2711) (cit. on p. 6).
- 32 [28] S Yi Zhou et al. "Substrate-induced bandgap opening in epitaxial graphene". In: *Nature
33 materials* 6.10 (2007), pp. 770–775 (cit. on p. 6).
- 34 [29] Edward McCann. "Asymmetry gap in the electronic band structure of bilayer graphene". In:
35 *Physical Review B* 74.16 (2006), p. 161403 (cit. on p. 6).
- 36 [30] Eduardo V Castro et al. "Biased bilayer graphene: semiconductor with a gap tunable
37 by the electric field effect". In: *Physical review letters* 99.21 (2007), p. 216802 (cit. on
38 p. 6).
- 39 [31] D. C. Elias et al. "Control of Graphene's Properties by Reversible Hydrogenation: Evi-
40 dence for Graphane". In: *Science* 323.5914 (2009), pp. 610–613. DOI: [10.1126/science.1167130](https://doi.org/10.1126/science.1167130) (cit. on pp. 6, 7).

- [32] Ki-Joon Jeon et al. "Fluorographene: A Wide Bandgap Semiconductor with Ultraviolet Luminescence". In: *ACS Nano* 5.2 (2011). PMID: 21204572, pp. 1042–1046. DOI: [10.1021/nn1025274](https://doi.org/10.1021/nn1025274) (cit. on pp. 6, 7). 1
2
3
- [33] SY Zhou et al. "Metal to insulator transition in epitaxial graphene induced by molecular doping". In: *Physical review letters* 101.8 (2008), p. 086402 (cit. on p. 6). 4
5
- [34] Kyoko Nakada et al. "Edge state in graphene ribbons: Nanometer size effect and edge shape dependence". In: *Phys. Rev. B* 54 (24 Dec. 1996), pp. 17954–17961. DOI: [10.1103/PhysRevB.54.17954](https://doi.org/10.1103/PhysRevB.54.17954) (cit. on p. 6). 6
7
8
- [35] Verónica Barone, Oded Hod, and Gustavo E. Scuseria. "Electronic Structure and Stability of Semiconducting Graphene Nanoribbons". In: *Nano Letters* 6.12 (2006). PMID: 17163699, pp. 2748–2754. DOI: [10.1021/nl0617033](https://doi.org/10.1021/nl0617033) (cit. on p. 6). 9
10
11
- [36] Zhiqiang Yang et al. "Birch Reduction of Graphite. Edge and Interior Functionalization by Hydrogen". In: *Journal of the American Chemical Society* 134.45 (2012). PMID: 23072630, pp. 18689–18694. DOI: [10.1021/ja3073116](https://doi.org/10.1021/ja3073116) (cit. on p. 7). 12
13
14
- [37] James S. Burgess et al. "Tuning the electronic properties of graphene by hydrogenation in a plasma enhanced chemical vapor deposition reactor". In: *Carbon* 49.13 (2011), pp. 4420–4426. DOI: [10.1016/j.carbon.2011.06.034](https://doi.org/10.1016/j.carbon.2011.06.034) (cit. on p. 7). 15
16
17
- [38] Yu Wang et al. "Toward high throughput interconvertible graphane-to-graphene growth and patterning". In: *ACS nano* 4.10 (2010), pp. 6146–6152 (cit. on p. 7). 18
19
- [39] Duminda K. Samarakoon and Xiao-Qian Wang. "Chair and Twist-Boat Membranes in Hydrogenated Graphene". In: *ACS Nano* 3.12 (2009). PMID: 19947580, pp. 4017–4022. DOI: [10.1021/nn901317d](https://doi.org/10.1021/nn901317d) (cit. on p. 7). 20
21
22
- [40] A.M. Illyin et al. "Computer simulation and experimental study of graphane-like structures formed by electrolytic hydrogenation". In: *Physica E: Low-dimensional Systems and Nanostructures* 43.6 (2011), pp. 1262–1265. DOI: [10.1016/j.physe.2011.02.012](https://doi.org/10.1016/j.physe.2011.02.012) (cit. on p. 7). 23
24
25
26
- [41] Enrique Muñoz et al. "The ultimate diamond slab: GraphAne versus graphEne". In: *Diamond and Related Materials* 19.5-6 (2010). Proceedings of Diamond 2009, The 20th European Conference on Diamond, Diamond-Like Materials, Carbon Nanotubes and Nitrides, Part 1, pp. 368–373. DOI: [10.1016/j.diamond.2010.01.007](https://doi.org/10.1016/j.diamond.2010.01.007) (cit. on p. 7). 27
28
29
30
- [42] J. Zhou et al. "Ferromagnetism in Semihydrogenated Graphene Sheet". Undetermined. In: *Nano Letters* 9.11 (Nov. 2009), pp. 3867–3870. DOI: [10.1021/nl9020733](https://doi.org/10.1021/nl9020733) (cit. on p. 7). 31
32
- [43] A. I. Shkrebtii et al. "Graphene and graphane functionalization with hydrogen: electronic and optical signatures". In: *physica status solidi (c)* 9.6 (2012), pp. 1378–1383. DOI: [10.1002/pssc.201100705](https://doi.org/10.1002/pssc.201100705) (cit. on p. 7). 33
34
35
- [44] Jorge O. Sofo, Ajay S. Chaudhari, and Greg D. Barber. "Graphane: A two-dimensional hydrocarbon". In: *Phys. Rev. B* 75 (15 Apr. 2007), p. 153401. DOI: [10.1103/PhysRevB.75.153401](https://doi.org/10.1103/PhysRevB.75.153401) (cit. on p. 8). 36
37
38
- [45] O Leenaerts et al. "First-principles investigation of graphene fluoride and graphane". In: *Physical Review B* 82.19 (2010), p. 195436 (cit. on p. 8). 39
40
- [46] Mingshan Zhu et al. "Fluorographene nanosheets with broad solvent dispersibility and their applications as a modified layer in organic field-effect transistors". In: *Phys. Chem. Chem. Phys.* 15 (48 2013), pp. 20992–21000. DOI: [10.1039/C3CP53383B](https://doi.org/10.1039/C3CP53383B) (cit. on pp. 7, 8). 41
42
43
44

- 1 [47] Duminda K. Samarakoon et al. "Structural and Electronic Properties of Fluorographene". In: *Small* 7.7 (Apr. 2011), pp. 965–969. DOI: [10.1002/smll.201002058](https://doi.org/10.1002/smll.201002058) (cit. on p. 7).
- 2
- 3 [48] Rahul R Nair et al. "Fluorographene: A Two-Dimensional Counterpart of Teflon". In: *small* 6.24 (2010), pp. 2877–2884 (cit. on pp. 7, 8).
- 4
- 5 [49] Chun-Liang Lin et al. "Substrate-Induced Symmetry Breaking in Silicene". In: *Phys. Rev. Lett.* 110 (7 Feb. 2013), p. 076801. DOI: [10.1103/PhysRevLett.110.076801](https://doi.org/10.1103/PhysRevLett.110.076801) (cit. on pp. 8, 9).
- 6
- 7 [50] Lars Matthes, Olivia Pulci, and Friedhelm Bechstedt. "Massive Dirac quasiparticles in
8 the optical absorbance of graphene, silicene, germanene, and tinene". In: *Journal of Physics: Condensed Matter* 25.39 (2013), p. 395305 (cit. on p. 9).
- 9
- 10 [51] Sivacarendran Balendhran et al. "Elemental Analogues of Graphene: Silicene, Germanene,
11 Stanene, and Phosphorene". In: *Small* 11.6 (2015), pp. 640–652. DOI: [10.1002/smll.201402041](https://doi.org/10.1002/smll.201402041) (cit. on p. 9).
- 12
- 13 [52] Joelson C. Garcia et al. "Group IV Graphene- and Graphane-Like Nanosheets". In: *The Journal of Physical Chemistry C* 115.27 (2011), pp. 13242–13246. DOI: [10.1021/jp203657w](https://doi.org/10.1021/jp203657w) (cit. on p. 9).
- 14
- 15 [53] Aaditya Manjanath, Vijay Kumar, and Abhishek K. Singh. "Mechanical and electronic
16 properties of pristine and Ni-doped Si, Ge, and Sn sheets". In: *Phys. Chem. Chem. Phys.* 16 (4 2014), pp. 1667–1671. DOI: [10.1039/C3CP54655A](https://doi.org/10.1039/C3CP54655A) (cit. on p. 9).
- 17
- 18 [54] Patrick Vogt et al. "Silicene: compelling experimental evidence for graphenelike two-
19 dimensional silicon". In: *Physical review letters* 108.15 (2012), p. 155501 (cit. on p. 10).
- 20
- 21 [55] Linfei Li et al. "Buckled germanene formation on Pt (111)". In: *Advanced Materials* 26.28 (2014), pp. 4820–4824 (cit. on p. 10).
- 22
- 23 [56] Chun-Liang Lin et al. "Structure of silicene grown on Ag (111)". In: *Applied Physics Express* 5.4 (2012), p. 045802 (cit. on p. 10).
- 24
- 25 [57] Thaneshwar P Kaloni and Udo Schwingenschlögl. "Weak interaction between germanene
26 and GaAs (0001) by H intercalation: a route to exfoliation". In: *Journal of Applied Physics* 114.18 (2013), p. 184307 (cit. on p. 10).
- 27
- 28 [58] Nasim Alem et al. "Atomically thin hexagonal boron nitride probed by ultrahigh-resolution
29 transmission electron microscopy". In: *Physical Review B* 80.15 (2009), p. 155425 (cit.
30 on p. 10).
- 31
- 32 [59] Houlong L Zhuang and Richard G Hennig. "Electronic structures of single-layer boron
33 pnictides". In: *Applied Physics Letters* 101.15 (2012), p. 153109 (cit. on p. 10).
- 34
- 35 [60] Alexey Bosak et al. "Elasticity of hexagonal boron nitride: Inelastic x-ray scattering mea-
36 surements". In: *Phys. Rev. B* 73 (4 Jan. 2006), p. 041402. DOI: [10.1103/PhysRevB.73.041402](https://doi.org/10.1103/PhysRevB.73.041402) (cit. on p. 10).
- 37
- 38 [61] Insun Jo et al. "Thermal Conductivity and Phonon Transport in Suspended Few-Layer
39 Hexagonal Boron Nitride". In: *Nano Letters* 13.2 (2013). PMID: 23346863, pp. 550–554.
DOI: [10.1021/nl304060g](https://doi.org/10.1021/nl304060g) (cit. on p. 10).
- 40
- 41 [62] Lu Hua Li and Ying Chen. "Atomically Thin Boron Nitride: Unique Properties and Ap-
42 plications". In: *Advanced Functional Materials* 26.16 (Apr. 2016), pp. 2594–2608. DOI:
[10.1002/adfm.201504606](https://doi.org/10.1002/adfm.201504606) (cit. on p. 10).

- [63] Gwan-Hyoung Lee et al. "Flexible and Transparent MoS₂ Field-Effect Transistors on Hexagonal Boron Nitride-Graphene Heterostructures". In: *ACS Nano* 7.9 (2013). PMID: 23924287, pp. 7931–7936. DOI: [10.1021/nn402954e](https://doi.org/10.1021/nn402954e) (cit. on p. 10).
1
2
3
- [64] DeanC R. et al. "Boron nitride substrates for high-quality graphene electronics". In: *Nat Nano* 5.10 (Oct. 2010), pp. 722–726. DOI: [10.1038/nano.2010.172](https://doi.org/10.1038/nano.2010.172) (cit. on p. 10).
4
5
- [65] via Wikimedia Commons Benjah-bmm27 (Own work) [Public domain]. *Boron-nitride-(hexagonal)-side-3D-balls*. 2007. URL: [https://commons.wikimedia.org/wiki/File%203ABoron-nitride-\(hexagonal\)-side-3D-balls.png](https://commons.wikimedia.org/wiki/File%203ABoron-nitride-(hexagonal)-side-3D-balls.png) (visited on 05/02/2017) (cit. on p. 11).
6
7
8
- [66] Qing Hua Wang et al. "Electronics and optoelectronics of two-dimensional transition metal dichalcogenides". In: *Nat. Nanotechnol.* 7.11 (Nov. 2012), pp. 699–712. DOI: [10.1038/nnano.2012.193](https://doi.org/10.1038/nnano.2012.193) (cit. on p. 11).
9
10
11
- [67] Z. Y. Zhu, Y. C. Cheng, and U. Schwingenschlögl. "Giant spin-orbit-induced spin splitting in two-dimensional transition-metal dichalcogenide semiconductors". In: *Phys. Rev. B* 84 (15 Oct. 2011), p. 153402. DOI: [10.1103/PhysRevB.84.153402](https://doi.org/10.1103/PhysRevB.84.153402) (cit. on p. 12).
12
13
14
- [68] Jaemyung Kim et al. "Enhanced Electrocatalytic Properties of Transition-Metal Dichalcogenides Sheets by Spontaneous Gold Nanoparticle Decoration". In: *The Journal of Physical Chemistry Letters* 4.8 (2013). PMID: 26282134, pp. 1227–1232. DOI: [10.1021/jz400507t](https://doi.org/10.1021/jz400507t) (cit. on p. 12).
15
16
17
18
- [69] Yunpeng Huang et al. "Synthesis of few-layered MoS₂ nanosheet-coated electrospun SnO₂ nanotube heterostructures for enhanced hydrogen evolution reaction". In: *Nanoscale* 6 (18 2014), pp. 10673–10679. DOI: [10.1039/C4NR02014F](https://doi.org/10.1039/C4NR02014F) (cit. on p. 12).
19
20
21
- [70] RadisavljevicB. et al. "Single-layer MoS₂ transistors". In: *Nat Nano* 6.3 (Mar. 2011), pp. 147–150. DOI: [10.1038/nnano.2010.279](https://doi.org/10.1038/nnano.2010.279) (cit. on p. 12).
22
23
- [71] Gengzhi Sun et al. "Fabrication of Ultralong Hybrid Microfibers from Nanosheets of Reduced Graphene Oxide and Transition-Metal Dichalcogenides and their Application as Supercapacitors". In: *Angewandte Chemie* 126.46 (2014), pp. 12784–12788. DOI: [10.1002/ange.201405325](https://doi.org/10.1002/ange.201405325) (cit. on p. 12).
24
25
26
27
- [72] Kun Chang and Weixiang Chen. "L-Cysteine-Assisted Synthesis of Layered MoS₂/Graphene Composites with Excellent Electrochemical Performances for Lithium Ion Batteries". In: *ACS Nano* 5.6 (2011). PMID: 21574610, pp. 4720–4728. DOI: [10.1021/nn200659w](https://doi.org/10.1021/nn200659w) (cit. on p. 12).
28
29
30
31
- [73] Dongyun Chen et al. "In situ nitrogenated graphene-few-layer WS₂ composites for fast and reversible Li⁺ storage". In: *Nanoscale* 5 (17 2013), pp. 7890–7896. DOI: [10.1039/C3NR02920D](https://doi.org/10.1039/C3NR02920D) (cit. on p. 12).
32
33
34
- [74] Yunguo Li et al. "Single-layer MoS₂ as an efficient photocatalyst". In: *Catal. Sci. Technol.* 3 (9 2013), pp. 2214–2220. DOI: [10.1039/C3CY00207A](https://doi.org/10.1039/C3CY00207A) (cit. on p. 12).
35
36
- [75] Eric Parzinger et al. "Photocatalytic Stability of Single- and Few-Layer MoS₂". In: *ACS Nano* 9.11 (2015). PMID: 26536283, pp. 11302–11309. DOI: [10.1021/acsnano.5b04979](https://doi.org/10.1021/acsnano.5b04979) (cit. on p. 12).
37
38
39
- [76] Liang Cheng et al. "PEGylated WS₂ Nanosheets as a Multifunctional Theranostic Agent for in vivo Dual-Modal CT/Photoacoustic Imaging Guided Photothermal Therapy". In: *Advanced Materials* 26.12 (2014), pp. 1886–1893. DOI: [10.1002/adma.201304497](https://doi.org/10.1002/adma.201304497) (cit. on p. 12).
40
41
42
43

- 1 [77] Wenyan Yin et al. "High-Throughput Synthesis of Single-Layer MoS₂ Nanosheets as
2 a Near-Infrared Photothermal-Triggered Drug Delivery for Effective Cancer Therapy".
3 In: *ACS Nano* 8.7 (2014). PMID: 24905027, pp. 6922–6933. DOI: [10.1021/nn501647j](https://doi.org/10.1021/nn501647j) (cit. on p. 12).
- 5 [78] Manish Chhowalla et al. "The chemistry of two-dimensional layered transition metal
6 dichalcogenide nanosheets". In: *Nat. Chem.* 5.4 (Mar. 2013), pp. 263–275. DOI: [10.1038/nchem.1589](https://doi.org/10.1038/nchem.1589) (cit. on p. 12).
- 8 [79] Jan Prasek et al. "Methods for carbon nanotubes synthesis-review". In: *J. Mater. Chem.*
9 21 (40 2011), pp. 15872–15884. DOI: [10.1039/C1JM12254A](https://doi.org/10.1039/C1JM12254A) (cit. on p. 13).
- 10 [80] Xinran Wang et al. "Room-Temperature All-Semiconducting Sub-10-nm Graphene Nanoribbons
11 Field-Effect Transistors". In: *Phys. Rev. Lett.* 100 (20 May 2008), p. 206803. DOI:
12 [10.1103/PhysRevLett.100.206803](https://doi.org/10.1103/PhysRevLett.100.206803) (cit. on p. 14).
- 13 [81] Melinda Y. Han et al. "Energy Band-Gap Engineering of Graphene Nanoribbons". In:
14 *Phys. Rev. Lett.* 98 (20 May 2007), p. 206805. DOI: [10.1103/PhysRevLett.98.206805](https://doi.org/10.1103/PhysRevLett.98.206805)
15 (cit. on p. 14).
- 16 [82] Young-Woo Son, Marvin L. Cohen, and Steven G. Louie. "Half-metallic graphene nanoribbons". In: *Nature* 444.7117 (), pp. 347–349. DOI: [10.1038/nature05180](https://doi.org/10.1038/nature05180) (cit. on p. 14).
- 18 [83] Prabhakar R. Bandaru. "Electrical Properties and Applications of Carbon Nanotube
19 Structures". In: *Journal of Nanoscience and Nanotechnology* 7.4-1(Apr. 2007), pp. 1239–
20 1267. DOI: [10.1166/jnn.2007.307](https://doi.org/10.1166/jnn.2007.307) (cit. on p. 14).
- 21 [84] Andrea C Ferrari et al. "Science and technology roadmap for graphene, related two-
22 dimensional crystals, and hybrid systems". In: *Nanoscale* 7.11 (2015), pp. 4598–4810.
23 DOI: [10.1039/C4NR01600A](https://doi.org/10.1039/C4NR01600A) (cit. on p. 15).
- 24 [85] Z. H. Ni et al. "On Resonant Scatterers As a Factor Limiting Carrier Mobility in Graphene"
25 In: *Nano Letters* 10.10 (2010). PMID: 20795655, pp. 3868–3872. DOI: [10.1021/nl101399r](https://doi.org/10.1021/nl101399r)
26 (cit. on p. 14).
- 27 [86] Neeraj Mishra et al. "Graphene growth on silicon carbide: A review". In: *physica status
28 solidi (a)* 213.9 (2016), pp. 2277–2289. DOI: [10.1002/pssa.201600091](https://doi.org/10.1002/pssa.201600091) (cit. on p. 16).
- 29 [87] Neeraj Mishra et al. "Graphene growth on silicon carbide: A review". In: *physica status
30 solidi (a)* 213.9 (Sept. 2016), pp. 2277–2289. DOI: [10.1002/pssa.201600091](https://doi.org/10.1002/pssa.201600091) (cit. on
31 p. 16).
- 32 [88] Nicholas Petrone et al. "Chemical Vapor Deposition-Derived Graphene with Electrical
33 Performance of Exfoliated Graphene". In: *Nano Letters* 12.6 (2012). PMID: 22582828,
34 pp. 2751–2756. DOI: [10.1021/nl204481s](https://doi.org/10.1021/nl204481s) (cit. on p. 17).
- 35 [89] Sukang Bae et al. "Roll-to-roll production of 30-inch graphene films for transparent
36 electrodes". In: *Nat Nano* 5.8 (Aug. 2010), pp. 574–578. DOI: [10.1038/nnano.2010.132](https://doi.org/10.1038/nnano.2010.132)
37 (cit. on p. 17).
- 38 [90] Scott Kirklin et al. "The Open Quantum Materials Database (OQMD): assessing the
39 accuracy of DFT formation energies". In: *npj Comput. Mater.* 1.1 (Dec. 2015), p. 15010.
40 DOI: [10.1038/npjcompumats.2015.10](https://doi.org/10.1038/npjcompumats.2015.10) (cit. on p. 19).
- 41 [91] P. Hohenberg and W. Kohn. "Inhomogeneous Electron Gas". In: *Phys. Rev.* 136 (3B Nov.
42 1964), B864–B871. DOI: [10.1103/PhysRev.136.B864](https://doi.org/10.1103/PhysRev.136.B864) (cit. on p. 19).

- [92] W. Kohn and L. J. Sham. "Self-Consistent Equations Including Exchange and Correlation Effects". In: *Phys. Rev.* 140 (4A Nov. 1965), A1133–A1138. DOI: [10.1103/PhysRev.140.A1133](https://doi.org/10.1103/PhysRev.140.A1133) (cit. on p. 19). 1
2
3
- [93] Neil Drummond. QMC Studies of Real Systems. 2017. URL: <http://slideplayer.com/slide/4763755/> (visited on 05/10/2017) (cit. on p. 20). 4
5
- [94] M. Born and R. Oppenheimer. "Zur Quantentheorie der Moleküle". In: *Annalen der Physik* 389.20 (1927), pp. 457–484. DOI: [10.1002/andp.19273892002](https://doi.org/10.1002/andp.19273892002) (cit. on p. 20). 6
7
- [95] Mel Levy. "Universal variational functionals of electron densities, first-order density matrices, and natural spin-orbitals and solution of the v-representability problem". In: *Proceedings of the National Academy of Sciences* 76.12 (1979), pp. 6062–6065. DOI: [10.1073/pnas.76.12.6062](https://doi.org/10.1073/pnas.76.12.6062) (cit. on p. 21). 8
9
10
11
- [96] John P Perdew. *Electronic structure of solids' 91*. Vol. 11. Akademie Verlag, Berlin, 1991 (cit. on p. 23). 12
13
- [97] John P. Perdew et al. "Atoms, molecules, solids, and surfaces: Applications of the generalized gradient approximation for exchange and correlation". In: *Phys. Rev. B* 46 (11 Sept. 1992), pp. 6671–6687. DOI: [10.1103/PhysRevB.46.6671](https://doi.org/10.1103/PhysRevB.46.6671) (cit. on p. 23). 14
15
16
- [98] John P. Perdew, Kieron Burke, and Matthias Ernzerhof. "Generalized Gradient Approximation Made Simple". In: *Phys. Rev. Lett.* 77 (18 Oct. 1996), pp. 3865–3868. DOI: [10.1103/PhysRevLett.77.3865](https://doi.org/10.1103/PhysRevLett.77.3865) (cit. on p. 23). 17
18
19
- [99] Qian Peng, Fernanda Duarte, and Robert S. Paton. "Computing organic stereoselectivity - from concepts to quantitative calculations and predictions". In: *Chem. Soc. Rev.* 45 (22 2016), pp. 6093–6107. DOI: [10.1039/C6CS00573J](https://doi.org/10.1039/C6CS00573J) (cit. on p. 24). 20
21
22
- [100] Carlo Adamo and Vincenzo Barone. "Toward reliable density functional methods without adjustable parameters: The PBE0 model". In: *The Journal of Chemical Physics* 110.13 (1999), pp. 6158–6170. DOI: [10.1063/1.478522](https://doi.org/10.1063/1.478522) (cit. on p. 23). 23
24
25
- [101] Jochen Heyd, Gustavo E. Scuseria, and Matthias Ernzerhof. "Hybrid functionals based on a screened Coulomb potential". In: *The Journal of Chemical Physics* 118.18 (2003), pp. 8207–8215. DOI: [10.1063/1.1564060](https://doi.org/10.1063/1.1564060) (cit. on p. 23). 26
27
28
- [102] M J Lucero, T M Henderson, and G E Scuseria. "Improved semiconductor lattice parameters and band gaps from a middle-range screened hybrid exchange functional". In: *Journal of Physics: Condensed Matter* 24.14 (2012), p. 145504. DOI: [10.1088/0953-8984/24/14/145504](https://doi.org/10.1088/0953-8984/24/14/145504) (cit. on p. 24). 29
30
31
32
- [103] David C. Langreth and John P. Perdew. "Theory of nonuniform electronic systems. I. Analysis of the gradient approximation and a generalization that works". In: *Phys. Rev. B* 21 (12 June 1980), pp. 5469–5493. DOI: [10.1103/PhysRevB.21.5469](https://doi.org/10.1103/PhysRevB.21.5469) (cit. on p. 25). 33
34
35
- [104] C. Fiolhais, F. Nogueira, and M.A.L. Marques. *A Primer in Density Functional Theory*. Lecture Notes in Physics. Springer-Verlag Berlin Heidelberg, 2003. DOI: [10.1007/3-540-37072-2](https://doi.org/10.1007/3-540-37072-2) (cit. on p. 26). 36
37
38
- [105] R. W. Godby, M. Schlüter, and L. J. Sham. "Self-energy operators and exchange-correlation potentials in semiconductors". In: *Phys. Rev. B* 37 (17 June 1988), pp. 10159–10175. DOI: [10.1103/PhysRevB.37.10159](https://doi.org/10.1103/PhysRevB.37.10159) (cit. on p. 25). 40
41
- [106] David Vanderbilt. "Soft self-consistent pseudopotentials in a generalized eigenvalue formalism". In: *Phys. Rev. B* 41 (11 Apr. 1990), pp. 7892–7895. DOI: [10.1103/PhysRevB.41.7892](https://doi.org/10.1103/PhysRevB.41.7892) (cit. on p. 28). 42
43
44

- [107] P. E. Blöchl. "Projector augmented-wave method". In: *Phys. Rev. B* 50 (24 Dec. 1994), pp. 17953–17979. DOI: [10.1103/PhysRevB.50.17953](https://doi.org/10.1103/PhysRevB.50.17953) (cit. on p. 28).
- [108] G. Kresse and D. Joubert. "From ultrasoft pseudopotentials to the projector augmented-wave method". In: *Phys. Rev. B* 59 (3 Jan. 1999), pp. 1758–1775. DOI: [10.1103/PhysRevB.59.1758](https://doi.org/10.1103/PhysRevB.59.1758) (cit. on p. 28).
- [109] *List of quantum chemistry and solid-state physics software*. 2017. URL: https://en.wikipedia.org/wiki/List_of_quantum_chemistry_and_solid-state_physics_software (visited on 05/15/2017) (cit. on p. 28).
- [110] Kurt Lejaeghere et al. "Reproducibility in density functional theory calculations of solids". In: *Science* 351.6280 (2016). DOI: [10.1126/science.aad3000](https://doi.org/10.1126/science.aad3000) (cit. on p. 28).
- [111] G. Kresse and J. Hafner. "Ab initio molecular-dynamics simulation of the liquid-metal-amorphous-semiconductor transition in germanium". In: *Phys. Rev. B* 49 (20 May 1994), pp. 14251–14269. DOI: [10.1103/PhysRevB.49.14251](https://doi.org/10.1103/PhysRevB.49.14251) (cit. on p. 28).
- [112] G. Kresse and J. Furthmüller. "Efficiency of ab-initio total energy calculations for metals and semiconductors using a plane-wave basis set". In: *Computational Materials Science* 6.1 (1996), pp. 15–50. DOI: [10.1016/0927-0256\(96\)00008-0](https://doi.org/10.1016/0927-0256(96)00008-0) (cit. on p. 28).
- [113] Johannes Diderik van der Waals. "Over de Continuiteit van den Gas- en Vloeistoftoestand (on the continuity of the gas and liquid state)". Ph.D. thesis. University of Leiden, 1873 (cit. on p. 29).
- [114] B. Partoens and F. M. Peeters. "From graphene to graphite: Electronic structure around the K point". In: *Phys. Rev. B* 74 (7 Aug. 2006), p. 075404. DOI: [10.1103/PhysRevB.74.075404](https://doi.org/10.1103/PhysRevB.74.075404) (cit. on pp. 30, 31).
- [115] Kin Fai Mak et al. "The evolution of electronic structure in few-layer graphene revealed by optical spectroscopy". In: *Proceedings of the National Academy of Sciences* 107.34 (2010), pp. 14999–15004. DOI: [10.1073/pnas.1004595107](https://doi.org/10.1073/pnas.1004595107) (cit. on p. 30).
- [116] R. Saito, G. Dresselhaus, and M.S. Dresselhaus. *Physical Properties of Carbon Nanotubes*. Imperial College Press, 1998 (cit. on p. 30).
- [117] K. F. Mak et al. "Atomically Thin MoS₂: A New Direct-Gap Semiconductor". In: *Physical Review Letters* 105.13, 136805 (Sept. 2010). [The version from arXiv.org], p. 136805. DOI: [10.1103/PhysRevLett.105.136805](https://doi.org/10.1103/PhysRevLett.105.136805) (cit. on p. 31).
- [118] C.A. Coulson and W.E. Moffitt. "I. The properties of certain strained hydrocarbons". In: *Phil. Mag.* 40.300 (1949), pp. 1–35. DOI: [10.1080/14786444908561208](https://doi.org/10.1080/14786444908561208) (cit. on p. 32).
- [119] Stock photo and royalty-free images on Fotolia.com - Pic 128894654. *sp3 sp2 sp hybrid orbitals*. 2016. URL: <https://www.fotolia.com/id/128894654> (visited on 05/25/2017) (cit. on p. 33).
- [120] Tobias Wassmann et al. "Clar's Theory, π -Electron Distribution, and Geometry of Graphene Nanoribbons". In: *J. Am. Chem. Soc.* 132.10 (Mar. 2010), pp. 3440–3451. DOI: [10.1021/ja909234y](https://doi.org/10.1021/ja909234y) (cit. on p. 34).
- [121] Thomson/Brooks Cole. *Double bond*. 2004. URL: http://images.slideplayer.com/14/4339766/slides/slide_7.jpg (visited on 04/21/2017) (cit. on p. 35).
- [122] Jinying Wang et al. "The rare two-dimensional materials with Dirac cones". In: *Natl. Sci. Rev.* 2.1 (Mar. 2015), pp. 22–39. DOI: [10.1093/nsr/nwu080](https://doi.org/10.1093/nsr/nwu080) (cit. on p. 36).

- [123] Yasumasa Hasegawa et al. "Zero modes of tight-binding electrons on the honeycomb lattice". In: *Phys. Rev. B* 74 (3 July 2006), p. 033413. DOI: [10.1103/PhysRevB.74.033413](https://doi.org/10.1103/PhysRevB.74.033413) (cit. on p. 36). 1
2
3
- [124] Zhirong Liu, Jinying Wang, and Jianlong Li. "Dirac cones in two-dimensional systems: from hexagonal to square lattices". In: *Phys. Chem. Chem. Phys.* 15 (43 2013), pp. 18855–18862. DOI: [10.1039/C3CP53257G](https://doi.org/10.1039/C3CP53257G) (cit. on p. 36). 4
5
6
- [125] G J Ackland, M C Warren, and S J Clark. "Practical methods in ab initio lattice dynamics". In: *J. Phys. Condens. Matter* 9.37 (Sept. 1997), pp. 7861–7872. DOI: [10.1088/0953-8984/9/37/017](https://doi.org/10.1088/0953-8984/9/37/017) (cit. on p. 37). 7
8
9
- [126] K. Parlinski. "Phonons calculated from first-principles". In: *École thématique la Société Française la Neutron*. 12 (June 2011), pp. 161–166. DOI: [10.1051/sfn/201112008](https://doi.org/10.1051/sfn/201112008) (cit. on p. 37). 10
11
12
- [127] Yongqing Cai et al. "Lattice vibrational modes and phonon thermal conductivity of monolayer MoS₂". In: *Phys. Rev. B* 89.3 (Jan. 2014), p. 035438. DOI: [10.1103/PhysRevB.89.035438](https://doi.org/10.1103/PhysRevB.89.035438) (cit. on p. 38). 13
14
15
- [128] Atsushi Togo and Isao Tanaka. "First principles phonon calculations in materials science". In: *Scripta Materialia* 108 (2015), pp. 1–5. DOI: <https://doi.org/10.1016/j.scriptamat.2015.07.021> (cit. on p. 40). 16
17
18
- [129] J.F. Nye. *Physical Properties of Crystals: Their Representation by Tensors and Matrices*. Oxford science publications. For example: Clarendon Press, 1985 (cit. on p. 40). 19
20

Draft - v1.0

Tuesday 30th May, 2017 – 17:32

Appendix A

1

Appendix

2